Published in final edited form as:

*Gene Ther*. 2022 April ; 29(3-4): 178–192. doi:10.1038/s41434-021-00303-4.

# Upper motor neurons are a target for gene therapy and UCHL1 is necessary and sufficient to improve cellular integrity of diseased upper motor neurons

**Barış Genç**[1,*], **Javier H. Jara**[1,*], **Santana S. Sanchez**[1], **Amiko K. B. Lagrimas**[1], **Oge Gozutok**[1], **Nuran Kocak**[1], **Yongling Zhu**[2], **P. Hande Özdinler**[1,#]

[1]Davee Department of Neurology and Clinical Neurological Sciences, Northwestern University, Feinberg School of Medicine, Chicago, IL, 60611

[2]Departments of Ophthalmology and Physiology, Feinberg School of Medicine, Northwestern University, Chicago, IL 60611

## Abstract

There are no effective cures for upper motor neuron (UMN) diseases, such as amyotrophic lateral sclerosis (ALS), primary lateral sclerosis, and hereditary spastic paraplegia. Here, we show UMN loss occurs independent of spinal motor neuron degeneration and that UMNs are indeed effective cellular targets for gene therapy, which offers a potential solution especially for UMN disease patients.

UCHL1 (ubiquitin C-terminal hydrolase-L1) is a deubiquitinating enzyme crucial for maintaining free ubiquitin levels. Corticospinal motor neurons (CSMN, a.k.a UMNs in mice) show early, selective, and profound degeneration in *Uchl1*$^{nm3419}$ (UCHL1$^{-/-}$) mice, which lack all UCHL1 function. When UCHL1 activity is ablated only from spinal motor neurons, CSMN remained intact. However, restoring UCHL1 specifically in CSMN of UCHL1$^{-/-}$ mice via directed gene delivery, was sufficient to improve CSMN integrity to the healthy control levels. In addition, when *UCHL1* gene was delivered selectively to CSMN that are diseased due to misfolded SOD1 toxicity and TDP-43 pathology via AAV-mediated retrograde transduction, the disease causing misfolded SOD1 and mutant human TDP-43 were reduced in hSOD1$^{G93A}$ and prpTDP-43$^{A315T}$ models, respectively. Diseased CSMN retained their neuronal integrity and cytoarchitectural stability in two different mouse models that represent two distinct causes of neurodegeneration in ALS.



#To whom correspondence should be addressed: P. Hande Ozdinler, ozdinler@northwestern.edu, Phone: (312) 503 2774, Fax: (312) 503 0872.

*These authors contributed equally

Author contributions

J.H.J., B.G., S.S.S., A.K.B.L., O.G., N.K., and P.H.O. performed experiments. J.H.J., B.G., S.S.S. and P.H.O. analyzed data, and J.H.J., B.G., and P.H.O. contributed to the writing of this manuscript.

Conflicts of interest

Authors have no competing interests to declare.

**Keywords**

CSMN; ALS; conditional mutant; gene therapy; spine density; SOD1; TDP-43

## INTRODUCTION

Motor neuron circuitry is one of the most complex circuitries in our body; it has important cellular and neuronal components both in the motor cortex and in the spinal cord and is responsible for the initiation and modulation of voluntary movement [1–3]. In motor neuron diseases, such as hereditary spastic paraplegia (HSP), primary lateral sclerosis (PLS) and amyotrophic lateral sclerosis (ALS), this complex circuitry degenerates [4–13]. There has been a long debate in the field about relevant contribution of different components of the circuitry so that targeted therapies can be developed [14–21]. Many argued that corticospinal motor neuron (CSMN) or the upper motor neuron (UMN) degeneration is a byproduct or a consequence of the "die-back" phenomenon [14–16]. This hypothesis unfortunately eliminated their importance and diminished enthusiasm of targeting UMNs as a cellular target even for UMN diseases [15].

Recent building evidence, however, began to reveal that UMNs degenerate early in diseases and the cortex is indeed a proper target for therapeutic interventions [1, 17–27]. Suppression of the mutant SOD1 only in the motor cortex was enough to delay disease onset in $SOD1^{G93A}$ rat model of ALS and extended their survival [28]. Transplantation of neural progenitor cells expressing GDNF into the motor cortex in $SOD1^{G93A}$ rat model of ALS provided neuroprotection in both motor cortex and spinal cord, delayed disease pathology and extended life span [29]. Cre-lox mediated ablation studies also confirmed that CSMN degeneration occurs via cell-autonomous mechanisms [30, 31]. In addition, cortical hyperexcitability is used as an early detection marker in ALS patients [1, 32–34]. Therefore, building evidence now reveal the importance of CSMN and UMN to disease pathology, and that they indeed are cellular targets for therapeutics [23, 24, 35].

UCHL1 is an important component of the ubiquitin-proteasome system (UPS) and can either add to or remove ubiquitin from polyubiquitin chains.[36–38] Mutations in *UCHL1* gene cause autosomal recessive spastic paraplegia-79 (SPG79) [39–43]. Patients develop spasticity with involvement of UMNs [39]. The $UCHL1^{-/-}$ mice, which lack all UCHL1 function [44], display motor function defects and progressive CSMN loss that accompanied by vacuolated apical dendrites, spine loss, and increased ER stress, which starts very early [45]. The spinal motor neurons (SMN) in these mice are also affected, and display disintegration of neuromuscular junctions (NMJ) [46]. Therefore, the same question arises: do CSMN degenerate because SMN are unhealthy? In an effort to develop gene therapy approaches selectively to UMNs, one must reveal whether CSMN degeneration is a function of SMN health, or whether CSMN health can be improved independently of SMN. $Rbp4^{cre}UCHL1^{f/f}$ and $HB9^{cre}UCHL1^{f/f}$ mice, which lack UCHL1 function only in large subcerebral projection neurons (SCPN) in layer 5, –which includes CSMN–, or in SMN in the spinal cord, offer great advantage to address this important issue. We find that CSMN

degeneration is not a function of SMN health and UMNs are indeed valid and effective cellular targets for gene therapy.

AAV2-mediated *UCHL1* gene delivery only to the CSMN of UCHL1$^{-/-}$ mice was sufficient to improve the cytoarchitectural integrity and stability of diseased CSMN, such that they become comparable to healthy CSMN. These results further prove the importance of UCHL1 for the health and integrity of UMNs and suggests *UCHL1* as a potential candidate for gene therapy for diseased UMNs. One of the cellular pathologies that is shared among many UMNs that become diseased due to different underlying causes, such as misfolded SOD1 toxicity [47–50], TDP-43 pathology [51, 52], lack of Alsin function [53], or mutations in the *profilin* gene [54], is disintegration of apical dendrite and spine loss. Interestingly, exactly the same pathology is detected in the Betz cells of a broad spectrum of ALS patients, including sALS, fALS and ALS/FTLD [9], UMNs in two different species display same cellular defects, suggesting that translation is at a cellular level and that improvement of CSMN health and stability will translate to UMN improvement in patients.

Here, we find that AAV-mediated *UCHL1* expression selectively in CSMN that are diseased due to mSOD1 toxicity and TDP-43 pathology, recovers their disease state, improves their neuronal integrity and stability, reduces their protein aggregation such that they become comparable to CSMN of healthy controls. hSOD1$^{G93A}$ and prpTDP-43$^{A315T}$ mice are one of the best characterized mouse models of ALS [47–52], and they recapitulate many aspects of ALS disease pathology, including progressive CSMN loss [47, 48, 51]. Yet, they represent different underlying causes of ALS and motor neuron degeneration [55–59].

Our findings show further proof that UMNs are indeed proper cellular targets for gene therapy approaches, especially for UMN diseases, and that their degeneration is not a function of SMN health. We also show evidence that direct delivery of UCHL1 to CSMN that become diseased due to mSOD1 toxicity and TDP-43 pathology is sufficient to improve their cytoarchitectural integrity and apical dendrite stability. Our results reveal *UCHL1* as a potential target for gene therapy approaches for diseased UMNs in ALS and other related motor neuron diseases.

## MATERIALS and METHODS

### Mice

All animal procedures were approved by Northwestern University Animal Care and Use Committee and conformed to the standards of the National Institutes of Health. *Uchl1*$^{nm3419}$ (UCHL1$^{-/-}$) mice carry a spontaneous 795 base-pair intragenic deletion that results in the removal of 24 base-pairs of exon 6 and 771 base-pairs of intron 6 [44–46]. Heterozygous mice (UCHL1$^{+/-}$) were viable, fertile, and bred to generate UCHL1 deficient (UCHL1$^{-/-}$) mice. Survival times and motor function defects were comparable between males and females with 100% penetrance. Uchl1$^{tm1a(EUCOMM)Hmgu}$ knockout first allele targeted embryonic stem cells were purchased from The European Conditional Mouse Mutagenesis (EUCOMM) Program. Floxed UCHL1 mice, in which exon 4 of the UCHL1 gene is flanked by *LoxP* sites, were generated with the assistance of Northwestern University Transgenic and Targeted Mutagenesis Laboratory. The lacZ/neo cassette flanked

by *FRT* sites in intron 3 was deleted by crossing germline transgenic mice with EIIa FLPeR mice (provided by Northwestern University Transgenic and Targeted Mutagenesis Laboratory), to generate the UCHL1$^{f/f}$ mice. Rbp4$^{cre}$ mice on a mixed background [Tg(Rbp4-cre)KL100Gsat/Mmucd; MMRRC stock# 031125-UCD] were purchased from Mutant Mouse Regional Resource Center (MMRRC) at UC Davis Mouse Biology Program [60–65]. HB9$^{cre}$ mice [B6.129S1-*Mnx1*$^{tm4(cre)Tmj}$/J; JAX stock #006600] were purchased from Jackson labs [66, 67]. Both floxed UCHL1 and Rbp4$^{cre}$ mouse lines were backcrossed to C57BL/6J background for at least 8 generations. Conditional mutant mice were generated by crossing floxed UCHL1 mice with Rbp4$^{cre}$ or HB9$^{cre}$ mice. hSOD1$^{G93A}$ mice expressing the high copy number of human SOD1 with the G93A point mutation were purchased from Jackson Labs (B6SJL-Tg(SOD1*G93A)1Gur/J; JAX stock # 002726) and backcrossed to C57BL/6J background in our laboratory [48, 50]. prpTDP-43$^{A315T}$ mice expressing the human TDP-43 with the A315T point mutation under the control of the prp promoter were purchased from Jackson Labs (B6.Cg-Tg(Prnp-TARDBP*A315T)95Balo/J; JAX stock # 010700) [51, 52]. Primers used to determine genotype of *Uchl1*$^{nm3419}$ mice are UCHL1 forward: tggacggctgtgtgtgctaatg, WT reverse: ctaagggaagggtcttgctcatc, mutant (Mt) reverse: gtcatctacctgaagagagccaag, yielding 668bp WT and 334bp Mt PCR products. Primers used to determine genotype of floxed UCHL1 mice are forward: tagtccaatccttgtaccagttgg and reverse: ccatggttctagatgctgttgaatgc, yielding 428 bp WT and 540 bp floxed UCHL1 products. Primers used to determine genotype of cre mice are forward: gcattaccggtcgatgcaacgagtgat and reverse: gagtgaacgaacctggtcgaaatcagt, yielding a 408 bp product. Primers used to determine genotype of hSOD1$^{G93A}$ mice are forward: catcagccctaatccatctga and reverse: cgcgactaacaatcaaag, yielding a 236 bp product. Primers used to determine genotype of prpTDP-43$^{A315T}$ mice are forward: ggatgagctgcgggagttct and reverse: tgcccatcatacccccaactg, yielding a 400 bp product.

## Generation of adeno-associated virus (AAV)

AAV vectors were generated by the University of Pennsylvania Vector Core facility by triple transfection of subconfluent HEK293 cells using three plasmids: an AAV trans-plasmid encoding AAV2 capsid, an adenovirus helper plasmid pΔF6, and an AAV cis shuttle plasmid expressing eGFP driven by a CMV promoter (pENN.AAV.CMV.PI.eGFP.WPRE.bGH). The culture medium was collected, concentrated by tangential flow filtration and purified by iodixanol gradient ultracentrifugation as previously described [68]. pGEM-T vector plasmid containing the mouse UCHL1 cDNA ORF clone was purchased from Sino Biological (cat: MG50690-G, Wayne, PA, USA), and the UCHL1 CDS was subcloned into a AAV plasmid with CBA promoter [69], to generate pAAV.CBA.UCHL1-IRES-eGFP.WPRE plasmid that was packaged into AAV2 virus particles by the University of Pennsylvania Vector Core facility as described above.

## Retrograde labeling and transduction surgeries

Surgeries were performed on a stereotaxic platform. Micro-injections were performed using pulled-beveled glass micro-pipettes attached to a nanojector (Drummond Scientific, Broomall, PA, USA). CSMN were retrogradely labeled by AAV encoding eGFP (AAV2-eGFP: 96 nl containing $4.88 \times 10^8$ genome copies; AAV2-UCHL1-IRES-eGFP: 414 nl containing $3.39 \times 10^9$ genome copies), injected into the CST and CSMN were retrogradely

transduced as described [45, 70]. Briefly, a small laminectomy at the cervical spinal cord (C2-C3) level was performed to expose the spinal cord, and to study cytoarchitecture of individual CSMN, a low dose of AAV is injected into the CST that lies within the dorsal funiculus (df) at 0.3 mm depth. This allows visualization of a subset of CSMN without too much overlap with neighboring cells, in a pattern similar to Golgi's silver stain, enabling detailed analysis of their morphology. To visualize maximum number of CSMN, 0.5% Fluoro-Gold (FG; Fluorochrome LLC, Denver, CO; 96nl in 0.9% saline solution) was injected as described. Mice were randomly assigned to receive either the AAV2-eGFP or AAV2-UCHL1-IRES-eGFP injections.

### Rotarod, hanging wire, and grip strength tests

Rotarod: A rotating rod that accelerates linearly from 4 to 40 rpm (Ugo Basile, Gemonio, VA, Italy) was used and an average time spent on the rotating rod for three consecutive trials was calculated for maximum 5 min. Hanging wire: Time each mouse spent hanging on to an upside-down wire mesh (50 cm above a bench) was recorded in 3 consecutive trials. Grip strength: Peak force applied by mice (forelimbs and hindlimbs recorded separately) was measured using grip strength meter (Ugo Basile, Gemonio, VA, Italy) in 3 consecutive trials.

### Tissue collection and histology

Mice were deeply anesthetized with ketamine (90 mg/kg) and xylazine (10 mg/kg) and perfused with 4% PFA in PBS. The brain was removed intact from each mouse, post-fixed by 4% PFA overnight and kept in PBS-sodium azide (0.01%) at 4°C. Brains were sectioned (coronal; 50 μm) using a vibrating microtome (VT1000S, Leica Instruments, Nussloch, Germany)

### Immunocytochemistry

Immunocytochemistry was performed on every 6$^{th}$ coronal section of mouse brains. Antigen retrieval was performed for Ctip2 immunocytochemistry; sections were treated with 0.01 M sodium citrate, pH 9.0, at 80°C water bath for 2 hr prior to incubation with primary antibody. Primary antibodies were: anti-Ctip2 (1:500; Abcam ab18465, Cambridge, MA, USA); anti-GFP (1:1000; Invitrogen A11122, Grand Island, NY, USA), anti-ChAT (1:200; Millipore AB144P, Burlington, MA, USA), anti-misfolded SOD1 (B8H10, 1:250, Médimabs MM-0070-P, Montreal, Quebec, Canada), anti-FLAG clone M2 (1:500, Sigma F1804, St. Louis, MO, USA), and anti-UCHL1 (1:1000; ProteinTech 14730-1-AP, Rosemont, IL, USA). After PBS washes, either fluorescent conjugated (AlexaFluor, Invitrogen, Grand Island, NY, USA) or biotinylated (Vector Laboratories, Burlingame, CA), USA secondary antibodies were used for detection.

### Quantification of misfolded SOD1 and TDP-43

50 μm thick free-floating sections of primary motor cortex were immunostained with the same antibody dilution at the same time. B8H10 monoclonal antibody can detect a wide spectrum of SOD1 mutants and metal-depleted WT SOD1 protein, but not intact WT SOD1 [71]. prpTDP-43$^{A315T}$ mice express the human TDP$^{A315T}$ protein with an N-terminal FLAG tag, therefore anti-FLAG antibody can be used to selectively visualize the exogenous

TDP-43$^{A315T}$ transgene product [52]. All images were captured using the 20X objective on an inverted epifluorescent Eclipse TE2000-E microscope (Nikon Inc., Melville, NY, USA) using the same settings and exposure time for all samples. Retrogradely labeled eGFP positive (eGFP$^{+}$) UMNs were traced using Image J (NIH, Bethesda, MD, USA). ROI were transferred to the B8H10 or FLAG channel, and the mean gray value was measured to determine the levels of misfolded SOD1 or human TDP$^{A315T}$ protein in GFP$^{+}$ UMNs only. All retrogradely labeled UMNs were included in the analysis, only UMNs with overlapping B8H10 or FLAG signal coming from other cells in other focal planes were excluded. Average mean gray value ± SEM was reported per experimental group.

### Imaging, quantification, and statistical analysis

Nikon SMZ1500 and Nikon Eclipse TE2000-E fluorescence microscopes equipped with Intensilight C-HGFI (Nikon Inc., Melville, NY, USA) were used. Epifluorescence images were acquired using a Digital Sight DS-Qi1MC CCD camera (Nikon Inc., Melville, NY, USA) and light images were acquired using a Ds-Fi1 camera (Nikon Inc., Melville, NY, USA). Confocal images were collected using a Zeiss 510 Meta confocal microscope (Carl Zeiss Inc., Thornwood, NY, USA). Numbers and diameters of CSMN were determined at P100. Since the AAV is injected into the CST and motor cortex is analyzed, the only cells that are labeled with this method are CSMN in layer 5 of primary motor cortex. Therefore, all cells with intact cell bodies were included in analysis regardless of their specific coordinates. Average CSMN diameter (at least 100 neurons / mouse; $n = 3$) was measured using Elements Software (Nikon Inc., Melville, NY, USA) OR Image J Software (NIH, Bethesda, MD, USA). For CSMN spine density measurements, a measured segment of apical dendrites (in layer 2/3, in the primary apical dendrite) were selected and the total numbers of spines were counted in each segment (10 segments/mouse; $n = 3$). The numbers were averaged, and results were presented as average number of spines per μm, per genotype. Even though all statistical analyses were performed per genotype, the information of the total counts are included in the results section to be informative on the extent of the quantitative assessment. All quantifications were performed blinded to the genotype and treatment of the mice.

Statistical analyses were based on the average numbers for each mouse, and not based on total individual number of counts. All statistical analyses were performed using Prism software (version 5.0a; Graphpad Software Inc., La Jolla, CA, USA). Statistically significant differences were determined after either one-way ANOVA with *post hoc* Tukey's multiple comparison tests or *t*-test. Statistically significant differences were considered at $p < 0.05$, and values were expressed as the mean ± SEM.

## RESULTS

### Site-specific *in vivo* deletion of UCHL1

To investigate the impact of the spinal motor neuron (SMN) dysfunction on CSMN cellular defects, and to assess the cell-autonomous importance of UCHL1 function for CSMN, we generated two conditional mutant mice, which lacked UCHL1 function either in CSMN or in SMN. First the floxed UCHL1 mice (UCHL1$^{f/f}$), in which the exon 4 of the *Uchl1* gene is

flanked by *loxP* sites, were generated (Fig. 1a). In the presence of cre recombinase, two *loxP* sites in introns 3 and 4 are recombined leading to deletion of *Uchl1* exon 4. This deletion introduces a *de novo* stop codon shortly after exon 3 in the *Uchl1* open reading frame (Fig. 1b), eliminating the production of a functional UCHL1 protein. Therefore, when UCHL1$^{f/f}$ mice were crossed with Rbp4$^{cre}$ mice, in which cre recombinase is expressed under the control of the Rbp4 promoter targeting SCPN (subcerebral projection neurons) in layer 5, –including the CSMN in the primary motor cortex–[60–63], UCHL1 is deleted from the CSMN in Rbp4$^{cre}$ UCHL1$^{f/f}$ mice (Fig. 1c). UCHL1$^{f/f}$ mice were also crossed with HB9$^{cre}$ [66, 67, 72–75] to generate the HB9$^{cre}$ UCHL1$^{f/f}$ mice, which lack UCHL1 protein in SMN but not in CSMN (Fig. 1c). These transgenic mice are generated to determine whether depletion of UCHL1 function in the SMN would have an impact on the health of CSMN.

CSMN can be identified their position in the layer 5 of primary motor cortex and expression of Ctip2 [2, 45, 48, 76, 77]. As expected, Ctip2$^{+}$ CSMN that normally have high levels of UCHL1 protein were not affected in the UCHL1$^{f/f}$ mice (Fig. 1d–d', e–e'), as CSMN continued to express endogenous UCHL1 at both postnatal day P30 and P100. However, even though UCHL1 expression was detected in other neurons within the motor column, CSMN completely lacked UCHL1 protein in the Rbp4$^{cre}$ UCHL1$^{f/f}$ mice (Fig. 1f–f', g–g'). In contrast, CSMN of HB9$^{cre}$ UCHL1$^{f/f}$ mice continued to express endogenous levels of UCHL1 and their levels were comparable to that of UCHL1$^{f/f}$ mice (Fig. 1h–h").

UCHL1 levels were not affected in SMN of UCHL1$^{f/f}$ mice (Fig. 2a–a', b–b'). In contrast, SMN of HB9$^{cre}$ UCHL1$^{f/f}$ mice lacked UCHL1 expression at both P30 and P100 (Fig. 2c–c', d–d'). Especially the large alpha motor neurons were devoid of UCHL1 expression in the ventral horn of the spinal cord (Fig. 2c'–d'). However, the SMN of the Rbp4$^{cre}$ UCHL1$^{f/f}$ mice continued to express UCHL1 even at P100 (Fig. 2e and e'), further confirming selective and robust deletion of UCHL1 in CSMN of the Rbp4$^{cre}$ UCHL1$^{f/f}$ mice and in SMN of HB9$^{cre}$ UCHL1$^{f/f}$ mice. It is also important to note that the absence of UCHL1 function did not affect the birth and specification of neither CSMN nor the SMN, as Ctip2$^{+}$ CSMN and ChAT$^{+}$ SMN were detected in both of these conditional mutant lines.

## CSMN defects in the absence of UCHL1 function are cell autonomous

CSMN were retrogradely transduced by AAV-2 eGFP, via injection into the corticospinal tract at P30 [2, 45, 70] and were analyzed at P100 (Fig. 3a). CSMN of UCHL1$^{f/f}$ control mice had large pyramidal cell bodies, prominent apical dendrites, and spines throughout the dendrites (Fig. 3b–d). The CSMN soma size (Fig. 3f) in UCHL1$^{-/-}$ (12.59 ± 0.22 μm, $n$ = 219 CSMN; $n$ = 9 mice) and Rbp4$^{cre}$ UCHL1$^{f/f}$ mice (13.35 ± 0.17 μm, $n$ = 469 CSMN; $n$ = 9 mice) were both significantly reduced when compared to the CSMN of UCHL1$^{f/f}$ mice (14.44 ± 0.19 μm, $n$ = 457 CSMN; $n$ = 9 mice; UCHL1$^{f/f}$ vs. UCHL1$^{-/-}$ $p$ = 0.0007; UCHL1$^{f/f}$ vs. Rbp4$^{cre}$ UCHL1$^{f/f}$ $p$ = 0.0052), but they were comparable to each other ($p$ = 0.2941). Interestingly, CSMN soma size in HB9$^{cre}$ UCHL1$^{f/f}$ mice (14.37 ± 0.21 μm, $n$ = 440 CSMN; $n$ = 13 mice) was comparable to that of CSMN in UCHL1$^{f/f}$ ($p$ = 0.9944), suggesting that deletion of UCHL1 in the SMN did not have impact on the overall health of CSMN.

We next investigated whether the integrity of apical dendrites was equally compromised in Rbp4$^{cre}$ UCHL1$^{f/f}$ and HB9$^{cre}$ UCHL1$^{f/f}$ mice. In line with previous reports, UCHL1$^{-/-}$ mice (81.16 ± 3.31%, $n$ = 357 apical dendrites, $n$ = 3 mice) exhibited significantly higher percentage of vacuolated CSMN apical dendrites (Fig. 3e) than CSMN of UCHL1$^{f/f}$ mice (26.08 ± 7.16%, $n$ = 654 apical dendrites, $n$ = 9 mice, $p$ = 0.0011). Majority of CSMN in Rbp4$^{cre}$ UCHL1$^{f/f}$ mice also had vacuolated apical dendrites (52.82 ± 7.29%, $n$ = 701 apical dendrites, $n$ = 11 mice; $p$ = 0.0235). Interestingly, CSMN of UCHL1$^{-/-}$ and Rbp4$^{cre}$ UCHL1$^{f/f}$ mice were comparable ($p$ = 0.1401). In contrast, CSMN of HB9$^{cre}$ UCHL1$^{f/f}$ mice, –which lacked UCHL1 only in the spinal cord, leaving UCHL1 intact in the brain–, displayed healthier morphology and percent apical dendrites with vacuoles were comparable to the CSMN of UCHL1$^{f/f}$ mice (23.68 ± 8.68%, $n$ = 842 apical dendrites, $n$ = 13 mice; $p$ = 0.992).

Spine numbers were reduced in apical dendrites that disintegrate. Average number of spines per μm of healthy primary apical dendrite (Fig. 4a) of the CSMN in UCHL1$^{f/f}$ (0.70 ± 0.15 spines/μm, $n$ = 3 mice), UCHL1$^{-/-}$ (0.63 ± 0.14 spines/μm, $n$ = 3 mice), Rbp4$^{cre}$ UCHL1$^{f/f}$ (0.87 ± 0.02 spines/μm, $n$ = 3 mice), and HB9$^{cre}$ UCHL1$^{f/f}$ mice (0.63 ± 0.07 spines/μm, $n$ = 3 mice) were comparable at P100 (Fig. 4b). Similarly, the average number of spines per μm of the vacuolated and disintegrating primary apical dendrite of the CSMN in UCHL1$^{f/f}$ (0.37 ± 0.01 spines/μm, $n$ = 3 mice), UCHL1$^{-/-}$ (0.35 ± 0.07 spines/μm, $n$ = 3 mice), Rbp4$^{cre}$ UCHL1$^{f/f}$ (0.38 ± 0.15 spines/μm, $n$ = 3 mice) and HB9$^{cre}$ UCHL1$^{f/f}$ mice (0.33 ± 0.03 spines/μm, $n$ = 3 mice) were similar (Fig. 4c). However, diseased apical dendrites always had reduced number of spines than healthy apical dendrites regardless of genotype. Since there is strong correlation between spine loss and the integrity of the apical dendrite [1, 9, 45, 51, 70, 78–83], for future quantitative assessments, we focused our attention to the health and integrity of the apical dendrite for each genotype and experimental condition.

## UCHL1 delivery to CSMN of UCHL1$^{-/-}$ mice is sufficient to improve CSMN integrity

We next took advantage of AAV2 mediated gene delivery to restore UCHL1 function only in the CSMN of UCHL1$^{-/-}$ mice (Fig. 5). AAV2 containing an UCHL1-IRES-eGFP bicistronic expression vector was injected into the corticospinal tract (CST) of UCHL1$^{-/-}$ mice at P30 and CSMN were analyzed at P100 (Fig. 5a). Wild type (WT) and UCHL1$^{-/-}$ mice that underwent same retrograde transduction surgery using the AAV2-GFP vector alone that does not contain the UCHL1 coding sequence were used as positive and negative controls, respectively. WT CSMN transduced by AAV2-eGFP express endogenous UCHL1 (Fig. 5b,e). UCHL1 protein is not detected in UCHL1$^{-/-}$ mice, and CSMN that are transduced with AAV2-eGFP also lack UCHL1 expression (Fig. 5c,f). In contrast, when CSMN are retrogradely transduced with AAV2-UCHL1-IRES-eGFP, which leads to the expression of both GFP and UCHL1 proteins, high level of UCHL1 expression is detected only in GFP$^{+}$ transduced CSMN (Fig. 5d,g), confirming effective transduction and directed gene delivery only to CSMN. AAV2-UCHL1-IRES-eGFP induces both UCHL1 and eGFP expression (not a fusion protein due to the bicistronic expression vector containing the IRES between two coding sequences), and because eGFP expression can be detected throughout the neuron, the integrity of the apical dendrites can be precisely assessed (Fig. 5b–d). Apical dendrites of WT mice were intact (Fig. 5b), but the apical dendrites of UCHL1$^{-/-}$ mice were mostly

filled with vacuoles (Fig. 5c). Interestingly, upon direct UCHL1 delivery to the CSMN, the integrity of the apical dendrites was dramatically improved; vacuolization of the apical dendrites was reduced and at times completely eliminated (Fig. 5d).

We used anti-GFP immunohistochemistry with DAB substrate to amplify GFP signal allowing precise analysis of retrogradely transduced CSMN (Fig. 6, Supplementary Fig. 1a). Using a low dose of AAV for retrograde transduction, enabled labeling only a small subset of CSMN with minimal overlap, –generating a pattern similar to Golgi's silver stain–, allowing detailed visualization and investigation of their cellular morphology with precision [2, 45, 70]. CSMN of WT mice displayed healthy robust apical dendrites (22.57 ± 3.48 %, $n = 735$ apical dendrites, $n = 5$ mice), whereas CSMN of UCHL1$^{-/-}$ mice contained significantly higher percentages of vacuoles (81.16 ± 3.31 %, $n = 357$ apical dendrites, $n = 3$ mice; $p < 0.0001$; Fig. 6c and e). When CSMN in UCHL1$^{-/-}$ mice were transduced by AAV2-UCHL1-IRES-eGFP, the integrity of apical dendrites was improved and the percent apical dendrites with vacuoles were dramatically reduced (32.41 ± 4.59%, $n = 195$ apical dendrites, $n = 5$ mice), becoming similar and comparable to that of WT mice ($p = 0.2125$). They were significantly lower than that of UCHL1$^{-/-}$ that are transfected by AAV2-eGFP alone ($p < 0.0001$).

In addition, while the soma diameter of CSMN in UCHL1$^{-/-}$ mice were significantly smaller (12.59 ± 0.22 μm, $n = 457$ cell bodies, $n = 9$ mice) than that of WT mice (15.47 ± 0.19 μm, $n = 986$ cell bodies, $n = 5$ mice; $p = 0.0014$; Fig. 6 d and f), when UCHL1 expression was selectively introduced to the CSMN of UCHL1$^{-/-}$ mice, soma diameter was also restored (14.85 ± 0.50 μm, $n = 137$ cell bodies, $n = 5$ mice), to the WT levels ($p = 0.452$).

Since AAV-mediated retrograde transduction targets only a small subgroup of CSMN, this application is more suitable for investigation of changes that occur in CSMN at a cellular level. As expected, we did not observe any improvement in overall motor function, which is assessed by rotarod, hanging wire and grip strength tests (Supplementary Fig. 2, Supplementary Table1).

## UCHL1 expression restores cytoarchitectural integrity of CSMN with mSOD1 toxicity

Restoring UCHL1 expression in CSMN of UCHL1$^{-/-}$ mice is sufficient to improve their integrity. However, would UCHL1 expression also help improve the health of CSMN that degenerate due to other causes? CSMN of hSOD1$^{G93A}$ mice become vulnerable to degeneration very early in the disease and they display progressive degeneration with reduced soma size and apical dendrite degeneration [47–49]. To investigate whether overexpression of UCHL1 in CSMN that are diseased due to misfolded SOD1 would also improve their overall health, stability and cytoarchitectural integrity, we used the same AAV2 mediated gene delivery approach to deliver UCHL1 to CSMN that are diseased due to mutant SOD1 toxicity. The injections were performed at P60 and into the CST and CSMN were analyzed at P120 (Fig. 7a).

CSMN of WT mice displayed healthy robust apical dendrites (20.05 ± 4.33 %, $n = 325$ apical dendrites, $n = 3$ mice), whereas CSMN of hSOD1$^{G93A}$ mice had significantly higher

percentages of vacuoles (58.90 ± 4.22 %, $n$ = 341 apical dendrites, $n$ = 4 mice; $p$ < 0.0001; Fig. 7b–c). Overexpression of UCHL1 in CSMN of hSOD1$^{G93A}$ mice significantly improved cytoarchitectural integrity (16.18 ± 1.04 %, $n$ = 442 apical dendrites, $n$ = 6 mice; $p$ < 0.0001) and was comparable to that of WT CSMN ($p$ = 0.7394). Overexpression of UCHL1 was not toxic, as UCHL1 expression in WT CSMN further reduced percentage of vacuolated apical dendrites (4.31 ± 1.06 %, $n$ = 189 apical dendrites, $n$ = 4 mice; $p$ = 0.0095).

Soma diameter of CSMN in hSOD1$^{G93A}$ mice were significantly smaller (12.25 ± 0.37 μm, $n$ = 140 cell bodies, $n$ = 4 mice) than that of WT mice (15.40 ± 0.41 μm, $n$ = 94 cell bodies, $n$ = 3 mice; $p$ = 0.0012; Fig. 7d–e). When UCHL1 was overexpressed in the CSMN of hSOD1$^{G93A}$ mice, soma diameter was also restored (15.74 ± 0.40 μm, $n$ = 155 soma, $n$ = 7 mice, $p$ < 0.0001), similar to the size of CSMN in WT mice ($p$ = 0.9402). Expression of UCHL1 in healthy CSMN did not affect soma diameter (16.41 ± 0.41 μm, $n$ = 85 soma, $n$ = 5 mice, $p$ = 0.4056).

## UCHL1 expression in CSMN with TDP-43 pathology improves soma size and integrity of apical dendrite

TDP-43 pathology is one of the most common proteinopaties observed in a large population of ALS patients [84, 85]. Because cellular causes of CSMN degeneration are shared between UMNs in prpTDP-43$^{A315T}$ mice and ALS patients with TDP-43 pathology [51], and CSMN of prpTDP-43$^{A315T}$ mice display early CSMN loss [86], we next wanted to investigate whether expression of UCHL1 would also promote the health and integrity of CSMN that become diseased due to TDP-43 pathology, a pathology that is mostly excluded from ALS patients with SOD1 mutations [55, 56], at a cellular level. UCHL1 is selectively introduced to CSMN by AAV-mediated retrograde transduction at P60, an early symptomatic stage, and CSMN health is analyzed at P120 (Fig. 8a). We used the same cohort of WT mice as controls for both hSOD1$^{G93A}$ and prpTDP-43$^{A315T}$ mice. CSMN of prpTDP-43$^{A315T}$ mice contained significantly higher percentages of vacuolated dendrites compared to that of WT (68.34 ± 3.41 %, $n$ = 243 apical dendrites, $n$ = 4 mice; $p$ < 0.0001; Fig. 8b–c). Expression of UCHL1 in CSMN of prpTDP-43$^{A315T}$ mice significantly improved cytoarchitectural integrity of apical dendrites (12.90 ± 1.63 %, $n$ = 324 apical dendrites, $n$ = 4 mice; $p$ < 0.0001), such that they became comparable to that of WT CSMN ($p$ = 0.3238). Soma diameter of CSMN in prpTDP-43$^{A315T}$ mice were significantly smaller (13.24 ± 0.39 μm, $n$ = 99 soma, $n$ = 4 mice, $p$ = 0.0209; Fig. 8d–e). However, upon UCHL1 expression, the soma diameter of CSMN in prpTDP-43$^{A315T}$ mice were fully restored (17.29 ± 0.52 μm, $n$ = 90 soma, $n$ = 4 mice, $p$ < 0.0001).

## UCHL1 expression reduces both the levels of misfolded SOD1 and human TDP-43$^{A315T}$

Since overexpression of the mutant form of *SOD1* gene causes accumulation of misfolded SOD1 in hSOD1$^{G93A}$ mouse model of ALS, and this is one of the major underlying causes of CSMN degeneration, we next investigated whether UCHL1 expression would also reduce the levels of misfolded SOD1 in CSMN by using the well characterized B8H10 monoclonal antibody that can detect misfolded SOD1 protein in a wide spectrum of SOD1 mutants and metal-depleted WT SOD1 protein, but not intact WT SOD1 [49, 71]. CSMN of WT mice

did not have misfolded SOD1, as expected (Fig. 9a). However, CSMN of hSOD1$^{G93A}$ mice contained high levels of misfolded SOD1 (1272 ± 26 arbitrary units (au), $n$ = 844 CSMN, $n$ = 6 mice vs WT: 224 ± 17 au, $n$ = 1310 CSMN, $n$ = 3 mice; $p < 0.0001$; Fig. 9a,b). AAV2-UCHL1-IRES-eGFP significantly reduced levels of misfolded SOD1in CSMN that are transduced with AAV expressing the *UCHL1* gene (1123 ± 27 au, $n$ = 255 CSMN, $n$ = 5 mice; hSOD1$^{G93A}$ eGFP vs. hSOD1$^{G93A}$ UCHL1-IRES-eGFP $p = 0.004$; WT vs. hSOD1$^{G93A}$ UCHL1-IRES-eGFP $p < 0.0001$; Fig. 9a,b).

PrpTDP-43$^{A315T}$ mice are generated by expressing the human TDP-43 protein with the A315T point mutation fused to an N-terminal FLAG tag [52], and it is mostly detected in the nucleus. To investigate the presence of human TDP-43$^{A315T}$ protein in CSMN of the prpTDP-43$^{A315T}$ mice, we used the FLAG monoclonal antibody. CSMN of WT mice do not have any human TDP-43$^{A315T}$ protein, as expected (Fig. 9c). However, CSMN of prpTDP-43$^{A315T}$ mice had high levels of human TDP-43$^{A315T}$ (1041 ± 20 arbitrary units (au), $n$ = 1536 CSMN, $n$ = 4 mice vs WT: 494 ± 5 au, $n$ = 1239 CSMN, $n$ = 3 mice; $p < 0.0001$; Fig. 9c,d). AAV2-UCHL1-IRES-eGFP significantly reduced levels of human TDP-43$^{A315T}$, (866 ± 66 au, $n$ = 111 CSMN, $n$ = 3 mice; prpTDP-43$^{A315T}$ eGFP vs. prpTDP-43$^{A315T}$ UCHL1-IRES-eGFP $p = 0.0257$; WT vs. prpTDP-43$^{A315T}$ UCHL1-IRES-eGFP $p = 0.0006$; Fig. 9c,d).

## DISCUSSION

Our results show proof for the cell-autonomous mechanisms responsible for CSMN degeneration and reveal that their demise is not correlated to or is a byproduct of SMN health. UCHL1 expression is required and sufficient to restore CSMN cytoarchitectural integrity and neuronal stability in UCHL1$^{-/-}$ mice, regardless of SMN health. Most interestingly, AAV-mediated gene delivery of *UCHL1* directly to CSMN that become diseased due to mutant SOD1 toxicity or TDP-43 pathology, two distinct and non-overlapping causes of ALS in patients [55–58, 87, 88], also leads to significant improvement of CSMN stability, cytoarchitectural integrity and neuronal health, so much so that they become comparable to healthy control levels. Therefore, we not only show proof that improving UMN health in a cell-autonomous manner is a valid approach, but also identify *UCHL1* as a potential candidate for gene therapy to diseased UMNs.

In an effort to bring a mechanistic insight for the CSMN degeneration in the absence of UCHL1 function, and to investigate whether introduction of UCHL1 would be sufficient to improve the cellular integrity of CSMN, we first knocked out UCHL1 protein selectively in the large subcerebral projection neurons (SCPN) in layer 5 or in SMN in the spinal cord by mating floxed UCHL1 (UCHL1$^{f/f}$) mice with Rbp4$^{cre}$ or HB9$^{cre}$ mice respectively. Conditional knockout of UCHL1 only in SCPN, which had healthy SMN, replicated CSMN pathology observed in UCHL1$^{-/-}$ mice. Moreover, AAV2-mediated delivery of the UCHL1 only to CSMN was sufficient to improve their cytoarchitectural integrity in UCHL1$^{-/-}$ mice. Direct gene delivery of *UCHL1* only to CSMN in UCHL1$^{-/-}$ mice, results in almost complete rescue of their neuronal stability, integrity of apical dendrites and spine, even when the rest of the mouse including SMN lack UCHL1 function. Therefore, we find that CSMN

health or degeneration is not a function of SMN, and UMNs are indeed valid cellular targets for therapeutic interventions.

However, since the number of CSMN targeted by the AAV was kept intentionally small to allow individual analysis at a cellular level, it was not sufficient to show a functional improvement in motor behavior. Next step would be to deliver UCHL1 to as many CSMN as possible in the motor cortex either via direct cortex injection or by intrathecal injection, such that more effective and broader UCHL1 expression can be achieved. In these future studies the full extent of motor neuron circuitry with spinal cord and the neuromuscular junction needs to be investigated. Here, our goal was to focus on the cell biology of CSMN, and investigate the impact of *UCHL1* expression on cellular stability and integrity. Now that we find UCHL1 treatment improves CSMN health and morphology, further detailed therapeutic studies are required.

UCHL1 is a unique protein. It has the ability to add and remove ubiquitin from proteins, playing an important role for their function, relocation within the cell, and ultimately determination of their fate for recycling [36–38, 89]. UCHL1 function is required to ensure free ubiquitin levels are stable in cells, especially in neurons. The ubiquitin–proteasome system plays a fundamental role in maintaining protein homeostasis, which is a crucial factor in the development of motor neuron diseases [90]. Even though all neurons ubiquitously express UCHL1, the UMNs have high levels of UCHL1 throughout life.

Interestingly, mutations in the *UCHL1* gene, which is located on chromosome 4p13, resulted in numerous forms of neurodegeneration that affects movement. For example, autosomal recessive spastic paraplegia-79 (SPG79) is caused by homozygous or compound heterozygous mutation in the *UCHL1* gene [42]. $UCHL1^{GLU7ALA}$ missense mutation lies within the ubiquitin-binding domain of UCHL1 protein and leads to loss of hydrolase function [39]. Siblings homozygous for the mutation have spasticity with UMN dysfunction. Patients with other missense mutations, such as $UCHL1^{ARG178GLN}$ and $UCHL1^{ALA216ASP}$ developed spasticity and ataxia following child onset blindness [41]. The $UCHL1^{ALA216ASP}$ mutation was reported to be insoluble and nonfunctional, whereas the $UCHL1^{ARG178GLN}$ mutation leads to a 4-fold increase in the hydrolytic activity. Recently, a third family with two siblings carrying a deleterious homozygous splice-site variant had spasticity [40]. Two siblings with Gly210del deletion had visual impairment, progressive spasticity, weakness, atrophy of the lower legs and ataxia [43]. Clinical features of all these 10 patients with mutations in their *UCHL1* gene share early neurodegeneration with indications of UMN involvement.

Similar to patients with mutations in their *UCHL1* gene, mouse models of UCHL1, especially the $Uchl1^{nm3419}$ ($UCHL1^{-/-}$) mice used in this study lack all UCHL1 function and display early onset neurodegeneration, accompanied with spasticity, muscular atrophy and profound upper motor neuron degeneration with disintegrating apical dendrites and spine loss [44–46]. Therefore, we think $UCHL1^{-/-}$ mice offers a unique opportunity to investigate upper motor neuron degeneration.

Numerous mouse models are generated to mimic ALS disease pathology. The hSOD1$^{G93A}$ and the prpTDP-43$^{A315T}$ models are one of the best characterized mouse models of ALS, recapitulating many aspects of disease pathology [47, 48, 50–52, 80–83]. TDP-43 pathology is observed in the brains of about 95% of ALS patients [84] regardless of a mutation in the *TARDP* gene [85, 91] and is distinct from fALS patients with *SOD1* mutations [87]. Patients with *SOD1* mutations or the SOD1 mouse models do not have TDP-43 pathology in their brains [55–58, 88]. Therefore, these two models represent two distinct disease mechanisms and a broad spectrum of patients. Interestingly, CSMN of these mice undergo progressive degeneration, which starts early with apical dendrite degeneration and spine loss [70]. Regardless of specific genes and mutations, disruption of protein homeostasis and canonical pathways such as ER stress, protein ubiquitination and unfolded protein response seem to be a common underlying cause for ALS and other neurodegenerative diseases [92–95]. It is possible UCHL1 provides benefit in both hSOD1$^{G93A}$ and the prpTDP-43$^{A315T}$ models due to its important role in the UPS pathway clearing toxic misfolded proteins [36, 37, 96, 97].

CSMN are an important member for the cortical component of motor neuron circuitry [4–6, 12]. While their soma resides in layer 5 of the motor cortex, their apical dendrite extend towards upper layers and the axon innervate spinal cord targets, forming a connection between brain and the spinal [2]. Their apical dendrite is a critical site for proper modulation. Therefore, the integrity and the stability of the apical dendrite is paramount for UMN health and function [2, 48, 98, 99].

We recently discovered that Betz cells of sporadic ALS, familial ALS and ALS-Frontotemporal Dementia patients display massive apical dendrite degeneration [1, 9, 100], and this cellular pathology is shared among species and observed in CSMN of numerous well characterized mouse models of ALS, such as hSOD1$^{G93A}$ [47, 48, 70], TDP-43$^{A315T}$ [51, 52, 80, 83], hPFN1$^{G118V}$ [54], and Alsin$^{KO}$ mice [53]. Therefore, identification of a treatment strategy that improves cytoarchitectural integrity, apical dendrite stability and eliminate spine loss would be translational. In addition, investigation of CSMN's requirements for survival and improved health is of great importance, as this information is clinically relevant, and has the potential to exponentially improve the success rates of future clinical trials of motor neuron diseases in which upper motor neurons and the motor neuron circuitry are affected.

UCHL1 protein fused to the protein transduction domain of HIV-transactivating transduction protein (TAT-UCHL1) can transduce neurons after intraperitoneal (i.p.) injection into mice [101]. In a controlled cortical impact (CCI) injury model of post-traumatic brain injury, TAT-UCHL1 treatment improved function of the ubiquitin-proteasome pathway, decreased activation of autophagy after CCI, attenuated axonal injury and increased hippocampal neuronal survival after CCI [101]. During hypoxic injury, whereas pharmacologic inhibition of UCHL1 function exacerbates neuronal death induced by hypoxia, TAT-UCHL1 treatment provides neuroprotection [102]. In a mouse model of AD, TAT-UCHL1 restored synaptic function in hippocampal slices after oligomeric Aβ treatment, and improved retention of contextual learning in APP/PS1 mice upon i.p. injection [103]. Moreover, Aβ induced impairment of neurotrophin-mediated retrograde signaling can be rescued by increasing cellular UCHL1 levels upon TAT-UCHL1 treatment [104]. These, in combination with

our UCHL1 rescue data using AAV-mediated gene delivery of *UCHL1* directly to CSMN suggest that UCHL1 could potentially be a therapeutic agent for treatment of not only a wide variety of neurodegenerative diseases, but also other injuries such as TBI, hypoxia, and cerebral ischemia.

Taken together, our results reveal that CSMN degeneration occurs independently of SMN health. UMNs, which play a pivotal role for the initiation and modulation of movement, are indeed cellular targets for therapeutic interventions. We also report *UCHL1* as a potential candidate for gene therapy approaches, especially for diseased UMNs. Because UMNs in mice and UMNs in patients share the same underlying pathologies, building evidence suggests that improving the integrity and stability of UMNs at a cellular level will offer a therapeutic benefit for the motor neuron circuitry that degenerates in patients. Since mutant SOD1 toxicity and especially TDP-43 pathology are observed in a wide spectrum of ALS patients, our results suggest that directed gene delivery of *UCHL*1 to diseased UMNs could offer a novel therapeutic intervention strategy for a broad spectrum of diseases, such as ALS, HSP, and PLS.

## Supplementary Material

Refer to Web version on PubMed Central for supplementary material.

## ACKNOWLEDGEMENTS

We thank UPenn Viral Vector Core, Bill Goosens and Jolanta Topczewska microscopy at the Stanley Manne Research Institute Lurie Children's Microscopy and Imaging Facility for help with the confocal microscope.

FUNDING

This work was supported by grants from NIH-R01NS085161-01 (P.H.O.), NUCATS (P.H.O.), and Mitsubishi Tanabe Pharma Holdings America, Inc. (P.H.O.). The Northwestern University Transgenic and Targeted Mutagenesis Laboratory is partially supported by NIH grant CA60553 to the Robert H. Lurie Comprehensive Cancer Center at Northwestern University.

## REFERENCES

1. Geevasinga N, Menon P, Ozdinler PH, Kiernan MC, Vucic S. Pathophysiological and diagnostic implications of cortical dysfunction in ALS. Nature reviews Neurology. 2016;12(11):651–61. [PubMed: 27658852]
2. Jara JH, Genc B, Klessner JL, Ozdinler PH. Retrograde labeling, transduction, and genetic targeting allow cellular analysis of corticospinal motor neurons: implications in health and disease. Front Neuroanat. 2014;8:16. [PubMed: 24723858]
3. Lemon RN. Descending pathways in motor control. Annual review of neuroscience. 2008;31:195–218.
4. Brunet A, Stuart-Lopez G, Burg T, Scekic-Zahirovic J, Rouaux C. Cortical Circuit Dysfunction as a Potential Driver of Amyotrophic Lateral Sclerosis. Frontiers in neuroscience. 2020;14:363. [PubMed: 32410944]
5. McColgan P, Joubert J, Tabrizi SJ, Rees G. The human motor cortex microcircuit: insights for neurodegenerative disease. Nature reviews Neuroscience. 2020;21(8):401–15. [PubMed: 32555340]
6. Gunes ZI, Kan VWY, Ye X, Liebscher S. Exciting Complexity: The Role of Motor Circuit Elements in ALS Pathophysiology. Frontiers in neuroscience. 2020;14(573):573. [PubMed: 32625051]
7. Fink JK. Hereditary spastic paraplegia: clinico-pathologic features and emerging molecular mechanisms. Acta neuropathologica. 2013;126(3):307–28. [PubMed: 23897027]

8. Fink JK. Progressive spastic paraparesis: hereditary spastic paraplegia and its relation to primary and amyotrophic lateral sclerosis. Semin Neurol. 2001;21(2):199–207. [PubMed: 11442328]
9. Genc B, Jara JH, Lagrimas AK, Pytel P, Roos RP, Mesulam MM, et al. Apical dendrite degeneration, a novel cellular pathology for Betz cells in ALS. Sci Rep. 2017;7:41765. [PubMed: 28165465]
10. Udaka F, Kameyama M, Tomonaga M. Degeneration of Betz cells in motor neuron disease. A Golgi study. Acta neuropathologica. 1986;70(3–4):289–95. [PubMed: 2429495]
11. Brown RH Jr., Robberecht W Amyotrophic lateral sclerosis: pathogenesis. Semin Neurol 2001;21(2):131–9. [PubMed: 11442322]
12. Novarino G, Fenstermaker AG, Zaki MS, Hofree M, Silhavy JL, Heiberg AD, et al. Exome sequencing links corticospinal motor neuron disease to common neurodegenerative disorders. Science. 2014;343(6170):506–11. [PubMed: 24482476]
13. Lemon RN. The Cortical “Upper Motoneuron” in Health and Disease. Brain Sci. 2021;11(5).
14. Chou SM, Norris FH. Amyotrophic lateral sclerosis: lower motor neuron disease spreading to upper motor neurons. Muscle & nerve. 1993;16(8):864–9. [PubMed: 8332139]
15. Dadon-Nachum M, Melamed E, Offen D. The “dying-back” phenomenon of motor neurons in ALS. J Mol Neurosci. 2011;43(3):470–7. [PubMed: 21057983]
16. Fischer LR, Culver DG, Tennant P, Davis AA, Wang M, Castellano-Sanchez A, et al. Amyotrophic lateral sclerosis is a distal axonopathy: evidence in mice and man. Experimental neurology. 2004;185(2):232–40. [PubMed: 14736504]
17. Eisen A The Dying Forward Hypothesis of ALS: Tracing Its History. Brain Sci. 2021;11(3).
18. Eisen A, Kim S, Pant B. Amyotrophic lateral sclerosis (ALS): a phylogenetic disease of the corticomotoneuron? Muscle & nerve. 1992;15(2):219–24. [PubMed: 1549143]
19. Baker MR. ALS--dying forward, backward or outward? Nature reviews Neurology. 2014;10(11):660.
20. Piotrkiewicz M, Hausmanowa-Petrusewicz I. Amyotrophic lateral sclerosis: a dying motor unit? Frontiers in aging neuroscience. 2013;5:7. [PubMed: 23533375]
21. Wainger BJ, Brown RH, Jr. Amyotrophic Lateral Sclerosis: Fuel for the Corticofugal Feud. Annals of neurology. 2020;88(4):682–4. [PubMed: 32741003]
22. Eisen A, Weber M. The motor cortex and amyotrophic lateral sclerosis. Muscle & nerve. 2001;24(4):564–73. [PubMed: 11268031]
23. Vucic S, Cheah BC, Kiernan MC. Defining the mechanisms that underlie cortical hyperexcitability in amyotrophic lateral sclerosis. Experimental neurology. 2009;220(1):177–82. [PubMed: 19716820]
24. Vucic S, Cheah BC, Yiannikas C, Kiernan MC. Cortical excitability distinguishes ALS from mimic disorders. Clin Neurophysiol. 2011;122(9):1860–6. [PubMed: 21382747]
25. Geevasinga N, Howells J, Menon P, van den Bos M, Shibuya K, Matamala JM, et al. . Amyotrophic lateral sclerosis diagnostic index: Toward a personalized diagnosis of ALS. Neurology. 2019;92(6):e536–e47. [PubMed: 30709964]
26. Lacomis D, Gooch C. Upper motor neuron assessment and early diagnosis in ALS: Getting it right the first time. Neurology. 2019;92(6):255–6. [PubMed: 30635480]
27. Vucic S, Nicholson GA, Kiernan MC. Cortical hyperexcitability may precede the onset of familial amyotrophic lateral sclerosis. Brain : a journal of neurology. 2008;131(Pt 6):1540–50. [PubMed: 18469020]
28. Thomsen GM, Gowing G, Latter J, Chen M, Vit JP, Staggenborg K, et al. Delayed disease onset and extended survival in the SOD1G93A rat model of amyotrophic lateral sclerosis after suppression of mutant SOD1 in the motor cortex. The Journal of neuroscience : the official journal of the Society for Neuroscience. 2014;34(47):15587–600. [PubMed: 25411487]
29. Thomsen GM, Avalos P, Ma AA, Alkaslasi M, Cho N, Wyss L, et al. Transplantation of Neural Progenitor Cells Expressing Glial Cell Line-Derived Neurotrophic Factor into the Motor Cortex as a Strategy to Treat Amyotrophic Lateral Sclerosis. Stem Cells. 2018;36(7):1122–31. [PubMed: 29656478]

30. Scekic-Zahirovic J, Fischer M, Stuart-Lopez G, Burg T, Gilet J, Dirrig-Grosch S, et al. Evidence that corticofugal propagation of ALS pathology is not mediated by prion-like mechanism. Progress in neurobiology. 2021;200:101972. [PubMed: 33309802]

31. Burg T, Bichara C, Scekic-Zahirovic J, Fischer M, Stuart-Lopez G, Brunet A, et al. Absence of Subcerebral Projection Neurons Is Beneficial in a Mouse Model of Amyotrophic Lateral Sclerosis. Annals of neurology. 2020;88(4):688–702. [PubMed: 32588450]

32. Vucic S, Ziemann U, Eisen A, Hallett M, Kiernan MC. Transcranial magnetic stimulation and amyotrophic lateral sclerosis: pathophysiological insights. Journal of neurology, neurosurgery, and psychiatry. 2013;84(10):1161–70.

33. Menon P, Geevasinga N, Yiannikas C, Howells J, Kiernan MC, Vucic S. Sensitivity and specificity of threshold tracking transcranial magnetic stimulation for diagnosis of amyotrophic lateral sclerosis: a prospective study. Lancet neurology. 2015;14(5):478–84. [PubMed: 25843898]

34. Kiernan MC, Vucic S, Talbot K, McDermott CJ, Hardiman O, Shefner JM, et al. Improving clinical trial outcomes in amyotrophic lateral sclerosis. Nature reviews Neurology. 2021;17(2):104–18. [PubMed: 33340024]

35. Geevasinga N, Menon P, Sue CM, Kumar KR, Ng K, Yiannikas C, et al. Cortical excitability changes distinguish the motor neuron disease phenotypes from hereditary spastic paraplegia. Eur J Neurol. 2015;22(5):826–31, e57–8. [PubMed: 25683471]

36. Day IN, Thompson RJ. UCHL1 (PGP 9.5): neuronal biomarker and ubiquitin system protein. Progress in neurobiology. 2010;90(3):327–62. [PubMed: 19879917]

37. Bishop P, Rocca D, Henley JM. Ubiquitin C-terminal hydrolase L1 (UCH-L1): structure, distribution and roles in brain function and dysfunction. Biochem J. 2016;473(16):2453–62. [PubMed: 27515257]

38. Liu Y, Fallon L, Lashuel HA, Liu Z, Lansbury PT, Jr. The UCH-L1 gene encodes two opposing enzymatic activities that affect alpha-synuclein degradation and Parkinson's disease susceptibility. Cell. 2002;111(2):209–18. [PubMed: 12408865]

39. Bilguvar K, Tyagi NK, Ozkara C, Tuysuz B, Bakircioglu M, Choi M, et al. Recessive loss of function of the neuronal ubiquitin hydrolase UCHL1 leads to early-onset progressive neurodegeneration. Proceedings of the National Academy of Sciences of the United States of America. 2013;110(9):3489–94. [PubMed: 23359680]

40. Das Bhowmik A, Patil SJ, Deshpande DV, Bhat V, Dalal A. Novel splice-site variant of UCHL1 in an Indian family with autosomal recessive spastic paraplegia-79. J Hum Genet. 2018;63(8):927–33. [PubMed: 29735986]

41. Rydning SL, Backe PH, Sousa MML, Iqbal Z, Oye AM, Sheng Y, et al. Novel UCHL1 mutations reveal new insights into ubiquitin processing. Human molecular genetics. 2017;26(6):1217–8. [PubMed: 28334853]

42. Blackstone C Converging cellular themes for the hereditary spastic paraplegias. Current opinion in neurobiology. 2018;51:139–46. [PubMed: 29753924]

43. McMacken G, Lochmuller H, Bansagi B, Pyle A, Lochmuller A, Chinnery PF, et al. Behr syndrome and hypertrophic cardiomyopathy in a family with a novel UCHL1 deletion. Journal of neurology. 2020;267(12):3643–9. [PubMed: 32656641]

44. Walters BJ, Campbell SL, Chen PC, Taylor AP, Schroeder DG, Dobrunz LE, et al. Differential effects of Usp14 and Uch-L1 on the ubiquitin proteasome system and synaptic activity. Molecular and cellular neurosciences. 2008;39(4):539–48. [PubMed: 18771733]

45. Jara JH, Genc B, Cox GA, Bohn MC, Roos RP, Macklis JD, et al. Corticospinal Motor Neurons Are Susceptible to Increased ER Stress and Display Profound Degeneration in the Absence of UCHL1 Function. Cereb Cortex. 2015;25(11):4259–72. [PubMed: 25596590]

46. Genc B, Jara JH, Schultz MC, Manuel M, Stanford MJ, Gautam M, et al. Absence of UCHL 1 function leads to selective motor neuropathy. Ann Clin Transl Neurol. 2016;3(5):331–45. [PubMed: 27231703]

47. Ozdinler PH, Benn S, Yamamoto TH, Guzel M, Brown RH Jr., Macklis JD. Corticospinal motor neurons and related subcerebral projection neurons undergo early and specific neurodegeneration in hSOD1G(9)(3)A transgenic ALS mice. The Journal of neuroscience : the official journal of the Society for Neuroscience. 2011;31(11):4166–77. [PubMed: 21411657]

48. Yasvoina MV, Genc B, Jara JH, Sheets PL, Quinlan KA, Milosevic A, et al. eGFP expression under UCHL1 promoter genetically labels corticospinal motor neurons and a subpopulation of degeneration-resistant spinal motor neurons in an ALS mouse model. The Journal of neuroscience : the official journal of the Society for Neuroscience. 2013;33(18):7890–904. [PubMed: 23637180]

49. Genc B, Gozutok O, Kocak N, Ozdinler PH. The Timing and Extent of Motor Neuron Vulnerability in ALS Correlates with Accumulation of Misfolded SOD1 Protein in the Cortex and in the Spinal Cord. Cells. 2020;9(2).

50. Gurney ME, Pu H, Chiu AY, Dal Canto MC, Polchow CY, Alexander DD, et al. Motor neuron degeneration in mice that express a human Cu,Zn superoxide dismutase mutation. Science. 1994;264(5166):1772–5. [PubMed: 8209258]

51. Gautam M, Jara JH, Kocak N, Rylaarsdam LE, Kim KD, Bigio EH, et al. Mitochondria, ER, and nuclear membrane defects reveal early mechanisms for upper motor neuron vulnerability with respect to TDP-43 pathology. Acta neuropathologica. 2019;137(1):47–69. [PubMed: 30450515]

52. Wegorzewska I, Bell S, Cairns NJ, Miller TM, Baloh RH. TDP-43 mutant transgenic mice develop features of ALS and frontotemporal lobar degeneration. Proceedings of the National Academy of Sciences of the United States of America. 2009;106(44):18809–14. [PubMed: 19833869]

53. Gautam M, Jara JH, Sekerkova G, Yasvoina MV, Martina M, Ozdinler PH. Absence of alsin function leads to corticospinal motor neuron vulnerability via novel disease mechanisms. Human molecular genetics. 2016;25(6):1074–87. [PubMed: 26755825]

54. Fil D, DeLoach A, Yadav S, Alkam D, MacNicol M, Singh A, et al. Mutant Profilin1 transgenic mice recapitulate cardinal features of motor neuron disease. Human molecular genetics. 2017;26(4):686–701. [PubMed: 28040732]

55. Mackenzie IR, Bigio EH, Ince PG, Geser F, Neumann M, Cairns NJ, et al. Pathological TDP-43 distinguishes sporadic amyotrophic lateral sclerosis from amyotrophic lateral sclerosis with SOD1 mutations. Annals of neurology. 2007;61(5):427–34. [PubMed: 17469116]

56. Robertson J, Sanelli T, Xiao S, Yang W, Horne P, Hammond R, et al. Lack of TDP-43 abnormalities in mutant SOD1 transgenic mice shows disparity with ALS. Neuroscience letters. 2007;420(2):128–32. [PubMed: 17543992]

57. Maekawa S, Leigh PN, King A, Jones E, Steele JC, Bodi I, et al. TDP-43 is consistently co-localized with ubiquitinated inclusions in sporadic and Guam amyotrophic lateral sclerosis but not in familial amyotrophic lateral sclerosis with and without SOD1 mutations. Neuropathology. 2009;29(6):672–83. [PubMed: 19496940]

58. Neumann M, Kwong LK, Sampathu DM, Trojanowski JQ, Lee VM. TDP-43 proteinopathy in frontotemporal lobar degeneration and amyotrophic lateral sclerosis: protein misfolding diseases without amyloidosis. Archives of neurology. 2007;64(10):1388–94. [PubMed: 17923623]

59. Genc B, Gautam M, Gozutok O, Dervishi I, Sanchez S, Goshu GM, et al. Improving mitochondria and ER stability helps eliminate upper motor neuron degeneration that occurs due to mSOD1 toxicity and TDP-43 pathology. Clin Transl Med. 2021;11(2):e336. [PubMed: 33634973]

60. Gerfen CR, Paletzki R, Heintz N. GENSAT BAC cre-recombinase driver lines to study the functional organization of cerebral cortical and basal ganglia circuits. Neuron. 2013;80(6):1368–83. [PubMed: 24360541]

61. Kim J, Hughes EG, Shetty AS, Arlotta P, Goff LA, Bergles DE, et al. Changes in the Excitability of Neocortical Neurons in a Mouse Model of Amyotrophic Lateral Sclerosis Are Not Specific to Corticospinal Neurons and Are Modulated by Advancing Disease. The Journal of neuroscience : the official journal of the Society for Neuroscience. 2017;37(37):9037–53. [PubMed: 28821643]

62. Leone DP, Heavner WE, Ferenczi EA, Dobreva G, Huguenard JR, Grosschedl R, et al. Satb2 Regulates the Differentiation of Both Callosal and Subcerebral Projection Neurons in the Developing Cerebral Cortex. Cereb Cortex. 2015;25(10):3406–19. [PubMed: 25037921]

63. Woodworth MB, Greig LC, Liu KX, Ippolito GC, Tucker HO, Macklis JD. Ctip1 Regulates the Balance between Specification of Distinct Projection Neuron Subtypes in Deep Cortical Layers. Cell Rep. 2016;15(5):999–1012. [PubMed: 27117402]

64. Gong S, Doughty M, Harbaugh CR, Cummins A, Hatten ME, Heintz N, et al. Targeting Cre recombinase to specific neuron populations with bacterial artificial chromosome constructs. The

Journal of neuroscience : the official journal of the Society for Neuroscience. 2007;27(37):9817–23. [PubMed: 17855595]

65. Gong S, Zheng C, Doughty ML, Losos K, Didkovsky N, Schambra UB, et al. A gene expression atlas of the central nervous system based on bacterial artificial chromosomes. Nature. 2003;425(6961):917–25. [PubMed: 14586460]
66. Yang X, Arber S, William C, Li L, Tanabe Y, Jessell TM, et al. Patterning of muscle acetylcholine receptor gene expression in the absence of motor innervation. Neuron. 2001;30(2):399–410. [PubMed: 11395002]
67. Arber S, Han B, Mendelsohn M, Smith M, Jessell TM, Sockanathan S. Requirement for the homeobox gene Hb9 in the consolidation of motor neuron identity. Neuron. 1999;23(4):659–74. [PubMed: 10482234]
68. Lock M, Alvira M, Vandenberghe LH, Samanta A, Toelen J, Debyser Z, et al. Rapid, simple, and versatile manufacturing of recombinant adeno-associated viral vectors at scale. Hum Gene Ther. 2010;21(10):1259–71. [PubMed: 20497038]
69. Zhu Y, Xu J, Hauswirth WW, DeVries SH. Genetically targeted binary labeling of retinal neurons. The Journal of neuroscience : the official journal of the Society for Neuroscience. 2014;34(23):7845–61. [PubMed: 24899708]
70. Jara JH, Villa SR, Khan NA, Bohn MC, Ozdinler PH. AAV2 mediated retrograde transduction of corticospinal motor neurons reveals initial and selective apical dendrite degeneration in ALS. Neurobiology of disease. 2012;47(2):174–83. [PubMed: 22521461]
71. Gros-Louis F, Soucy G, Lariviere R, Julien JP. Intracerebroventricular infusion of monoclonal antibody or its derived Fab fragment against misfolded forms of SOD1 mutant delays mortality in a mouse model of ALS. Journal of neurochemistry. 2010;113(5):1188–99. [PubMed: 20345765]
72. Wichterle H, Lieberam I, Porter JA, Jessell TM. Directed differentiation of embryonic stem cells into motor neurons. Cell. 2002;110(3):385–97. [PubMed: 12176325]
73. Wilson JM, Hartley R, Maxwell DJ, Todd AJ, Lieberam I, Kaltschmidt JA, et al. Conditional rhythmicity of ventral spinal interneurons defined by expression of the Hb9 homeodomain protein. The Journal of neuroscience : the official journal of the Society for Neuroscience. 2005;25(24):5710–9. [PubMed: 15958737]
74. Kramer ER, Knott L, Su F, Dessaud E, Krull CE, Helmbacher F, et al. Cooperation between GDNF/Ret and ephrinA/EphA4 signals for motor-axon pathway selection in the limb. Neuron. 2006;50(1):35–47. [PubMed: 16600854]
75. Gogliotti RG, Quinlan KA, Barlow CB, Heier CR, Heckman CJ, Didonato CJ. Motor neuron rescue in spinal muscular atrophy mice demonstrates that sensory-motor defects are a consequence, not a cause, of motor neuron dysfunction. The Journal of neuroscience : the official journal of the Society for Neuroscience. 2012;32(11):3818–29. [PubMed: 22423102]
76. Molyneaux BJ, Arlotta P, Menezes JR, Macklis JD. Neuronal subtype specification in the cerebral cortex. Nature reviews Neuroscience. 2007;8(6):427–37. [PubMed: 17514196]
77. Molyneaux BJ, Arlotta P, Macklis JD. Molecular development of corticospinal motor neuron circuitry. Novartis Foundation symposium. 2007;288(2):3–15; discussion −20, 96–8. [PubMed: 18494249]
78. Fogarty MJ. Driven to decay: Excitability and synaptic abnormalities in amyotrophic lateral sclerosis. Brain research bulletin. 2018;140:318–33. [PubMed: 29870780]
79. Fogarty MJ. Amyotrophic lateral sclerosis as a synaptopathy. Neural Regen Res. 2019;14(2):189–92. [PubMed: 30530995]
80. Fogarty MJ, Klenowski PM, Lee JD, Drieberg-Thompson JR, Bartlett SE, Ngo ST, et al. Cortical synaptic and dendritic spine abnormalities in a presymptomatic TDP-43 model of amyotrophic lateral sclerosis. Sci Rep. 2016;6:37968. [PubMed: 27897242]
81. Fogarty MJ, Mu EW, Noakes PG, Lavidis NA, Bellingham MC. Marked changes in dendritic structure and spine density precede significant neuronal death in vulnerable cortical pyramidal neuron populations in the SOD1(G93A) mouse model of amyotrophic lateral sclerosis. Acta Neuropathol Commun. 2016;4(1):77. [PubMed: 27488828]
82. Fogarty MJ, Noakes PG, Bellingham MC. Motor cortex layer V pyramidal neurons exhibit dendritic regression, spine loss, and increased synaptic excitation in the presymptomatic

hSOD1(G93A) mouse model of amyotrophic lateral sclerosis. The Journal of neuroscience : the official journal of the Society for Neuroscience. 2015;35(2):643–7. [PubMed: 25589758]

83. Handley EE, Pitman KA, Dawkins E, Young KM, Clark RM, Jiang TC, et al. Synapse Dysfunction of Layer V Pyramidal Neurons Precedes Neurodegeneration in a Mouse Model of TDP-43 Proteinopathies. Cereb Cortex. 2017;27(7):3630–47. [PubMed: 27496536]
84. Ling SC, Polymenidou M, Cleveland DW. Converging mechanisms in ALS and FTD: disrupted RNA and protein homeostasis. Neuron. 2013;79(3):416–38. [PubMed: 23931993]
85. Cykowski MD, Powell SZ, Peterson LE, Appel JW, Rivera AL, Takei H, et al. Clinical Significance of TDP-43 Neuropathology in Amyotrophic Lateral Sclerosis. Journal of neuropathology and experimental neurology. 2017;76(5):402–13. [PubMed: 28521037]
86. Gautam M, Xie EF, Kocak N, Ozdinler PH. Mitoautophagy: A Unique Self-Destructive Path Mitochondria of Upper Motor Neurons With TDP-43 Pathology Take, Very Early in ALS. Front Cell Neurosci. 2019;13:489. [PubMed: 31787882]
87. Rosen DR, Siddique T, Patterson D, Figlewicz DA, Sapp P, Hentati A, et al. Mutations in Cu/Zn superoxide dismutase gene are associated with familial amyotrophic lateral sclerosis. Nature. 1993;362(6415):59–62. [PubMed: 8446170]
88. Robertson J, Sanelli T, Xiao SX, Yang WC, Horne P, Hammond R, et al. Lack of TDP-43 abnormalities in mutant SOD1 transgenic mice shows disparity with ALS. Neuroscience letters. 2007;420(2):128–32. [PubMed: 17543992]
89. Reinicke AT, Laban K, Sachs M, Kraus V, Walden M, Damme M, et al. Ubiquitin C-terminal hydrolase L1 (UCH-L1) loss causes neurodegeneration by altering protein turnover in the first postnatal weeks. Proceedings of the National Academy of Sciences of the United States of America. 2019;116(16):7963–72. [PubMed: 30923110]
90. Bachiller S, Alonso-Bellido IM, Real LM, Perez-Villegas EM, Venero JL, Deierborg T, et al. The Ubiquitin Proteasome System in Neuromuscular Disorders: Moving Beyond Movement. Int J Mol Sci. 2020;21(17).
91. Coan G, Mitchell CS. An Assessment of Possible Neuropathology and Clinical Relationships in 46 Sporadic Amyotrophic Lateral Sclerosis Patient Autopsies. Neuro-degenerative diseases. 2015;15(5):301–12. [PubMed: 26183171]
92. Dervishi I, Gozutok O, Murnan K, Gautam M, Heller D, Bigio E, et al. Protein-protein interactions reveal key canonical pathways, upstream regulators, interactome domains, and novel targets in ALS. Sci Rep. 2018;8(1):14732. [PubMed: 30283000]
93. Boland B, Yu WH, Corti O, Mollereau B, Henriques A, Bezard E, et al. Promoting the clearance of neurotoxic proteins in neurodegenerative disorders of ageing. Nat Rev Drug Discov. 2018;17(9):660–88. [PubMed: 30116051]
94. Turker F, Cook EK, Margolis SS. The proteasome and its role in the nervous system. Cell Chem Biol. 2021;28(7):903–17. [PubMed: 33905676]
95. Cicardi ME, Marrone L, Azzouz M, Trotti D. Proteostatic imbalance and protein spreading in amyotrophic lateral sclerosis. EMBO J. 2021;40(10):e106389. [PubMed: 33792056]
96. Graham SH, Liu H. Life and death in the trash heap: The ubiquitin proteasome pathway and UCHL1 in brain aging, neurodegenerative disease and cerebral Ischemia. Ageing Res Rev. 2017;34:30–8. [PubMed: 27702698]
97. Jara JH, Frank DD, Ozdinler PH. Could dysregulation of UPS be a common underlying mechanism for cancer and neurodegeneration? Lessons from UCHL1. Cell biochemistry and biophysics. 2013;67(1):45–53. [PubMed: 23695785]
98. Anderson CT, Sheets PL, Kiritani T, Shepherd GM. Sublayer-specific microcircuits of corticospinal and corticostriatal neurons in motor cortex. Nature neuroscience. 2010;13(6):739–44. [PubMed: 20436481]
99. Shepherd GM. Corticostriatal connectivity and its role in disease. Nature reviews Neuroscience. 2013;14(4):278–91. [PubMed: 23511908]
100. Jara JH, Genc B, Stanford MJ, Pytel P, Roos RP, Weintraub S, et al. Evidence for an early innate immune response in the motor cortex of ALS. J Neuroinflammation. 2017;14(1):129. [PubMed: 28651542]

101. Liu H, Rose ME, Ma X, Culver S, Dixon CE, Graham SH. In vivo transduction of neurons with TAT-UCH-L1 protects brain against controlled cortical impact injury. PloS one. 2017;12(5):e0178049. [PubMed: 28542502]

102. Liu H, Li W, Ahmad M, Miller TM, Rose ME, Poloyac SM, et al. Modification of ubiquitin-C-terminal hydrolase-L1 by cyclopentenone prostaglandins exacerbates hypoxic injury. Neurobiology of disease. 2011;41(2):318–28. [PubMed: 20933087]

103. Gong B, Cao Z, Zheng P, Vitolo OV, Liu S, Staniszewski A, et al. Ubiquitin hydrolase Uch-L1 rescues beta-amyloid-induced decreases in synaptic function and contextual memory. Cell. 2006;126(4):775–88. [PubMed: 16923396]

104. Poon WW, Carlos AJ, Aguilar BL, Berchtold NC, Kawano CK, Zograbyan V, et al. beta-Amyloid (Abeta) oligomers impair brain-derived neurotrophic factor retrograde trafficking by down-regulating ubiquitin C-terminal hydrolase, UCH-L1. The Journal of biological chemistry. 2013;288(23):16937–48. [PubMed: 23599427]

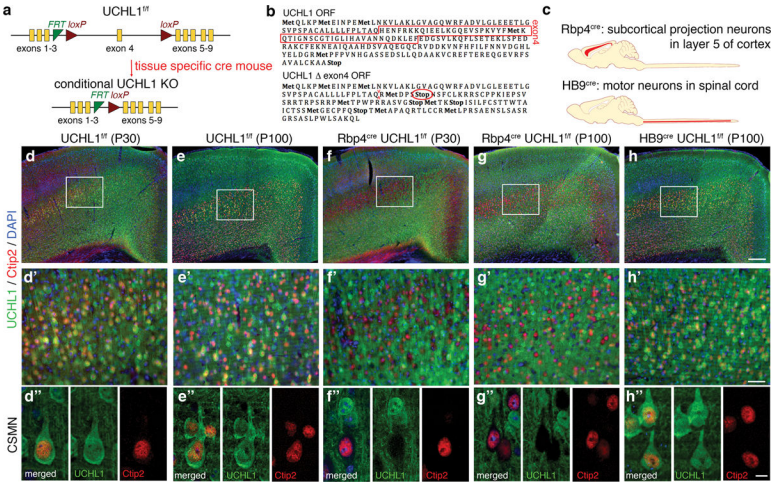


**Fig. 1: UCHL1 expression can be deleted using cre/lox conditional mutant approach in the CSMN of floxed UCHL1 mice.**

**a** Floxed UCHL1 (UCHL1$^{f/f}$) mice were generated by introducing *loxP* sites flanking the exon 4 of UCHL1. Cre recombinase activity leads to removal of the exon 4. **b** Deletion of exon 4 of mouse UCHL1 gene introduces a *de novo* stop codon shortly after the deletion site. **c** Rbp4$^{cre}$ mice drives the expression of cre recombinase in layer 5 subcortical projection neurons including the CSMN. HB9$^{cre}$ mice drives the expression of cre recombinase in spinal motor neurons located in the ventral horn of the spinal cord. Crossing these cre driver mice with UCHL1$^{f/f}$ mice leads to conditional mutant mice that lack UCHL1 function either in the CSMN or the SMN. **d-h** Representative images of primary motor cortex from UCHL1$^{f/f}$ (**d-e**), Rbp4$^{cre}$ UCHL1$^{f/f}$ (**f-g**), and HB9$^{cre}$ UCHL1$^{f/f}$ (**h**) mice at P30 (**d, f**) and P100 (**e, g, h**). CSMN can be identified by Ctip2$^{+}$ nuclei. Scale bars on top panel = 250 μm **d'-h'** Representative images of layer 5 of primary motor cortex from UCHL1$^{f/f}$ (**d'-e'**), Rbp4$^{cre}$ UCHL1$^{f/f}$ (**f'-g'**), and HB9$^{cre}$ UCHL1$^{f/f}$ (**h'**) mice at P30 (**d', f'**) and P100 (**e', g', h'**). Scale bar = 50 μm. **d"-h"** Representative images of CSMN from UCHL1$^{f/f}$ (**d"-e"**), Rbp4$^{cre}$ UCHL1$^{f/f}$ (**f"-g"**), and HB9$^{cre}$ UCHL1$^{f/f}$ (**h"**) mice at P30 (**d", f"**) and P100 (**e", g", h"**) captured by confocal microscope. Scale bar = 10 μm.

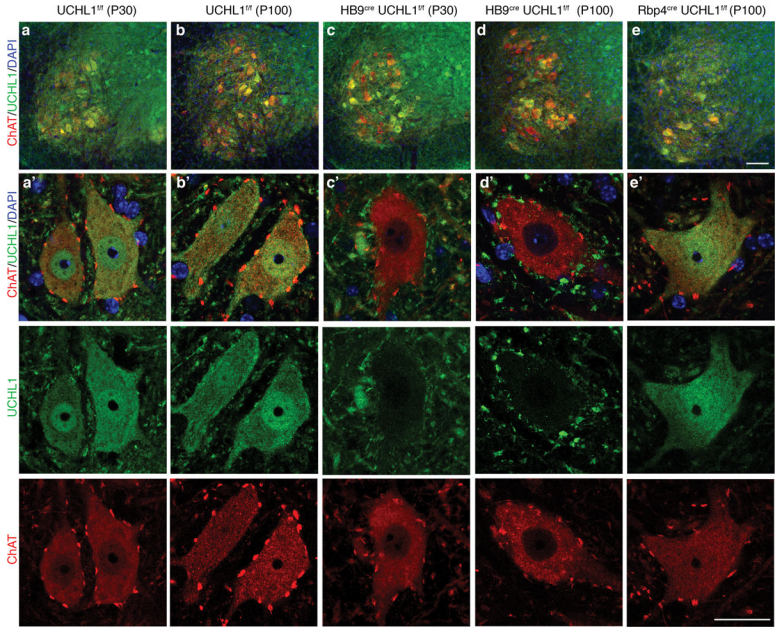


**Fig. 2: HB9$^{cre}$ UCHL1$^{f/f}$ mice lack UCHL1 in their spinal motor neurons (SMN)**

**a-e** Representative images of the ventral horn of the spinal cord of UCHL1$^{f/f}$ (**a-b),** HB9$^{cre}$ UCHL1$^{f/f}$ (**c-d),** and Rbp4$^{cre}$ UCHL1$^{f/f}$ (**e**) mice at P30 (**a, c**) and P100 (**b, d, e**). Scale bar = 100 μm. **a'-e'** Representative images of ChAT$^{+}$ SMN from UCHL1$^{f/f}$ (**a'-b'**), HB9$^{cre}$ UCHL1$^{f/f}$ (**c'-d'),** and Rbp4$^{cre}$ UCHL1$^{f/f}$ (**e'**) mice at P30 (**a', c'**) and P100 (**b', d', e'**) captured by confocal microscope. Scale bar = 20 μm.

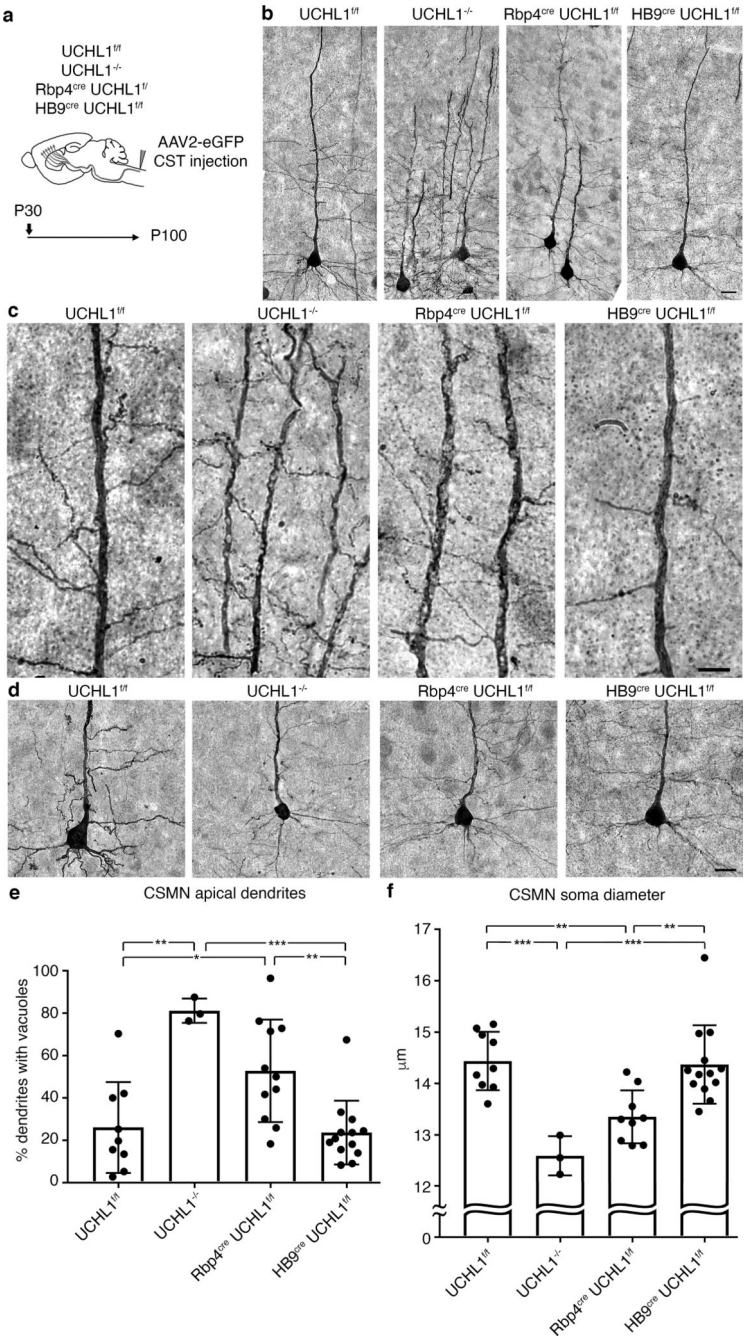


**Fig. 3: Cortex specific UCHL1 conditional mutant mice recapitulate pathology observed in the CSMN of UCHL1$^{-/-}$ mice.**

**a** Schematic overview of the experimental setup. CSMN of UCHL1$^{f/f}$, UCHL1$^{-/-}$, Rbp4$^{cre}$ UCHL1$^{f/f}$, and HB9$^{cre}$ UCHL1$^{f/f}$ mice were retrogradely transduced by injecting AAV2-eGFP into the corticospinal tract (CST) at P30, and CSMN were analyzed at P100. **b** Representative images of GFP labeled CSMN after DAB mediated immunohistochemistry enhancement of the GFP signal allowing investigation of CSMN morphology in detail. Scale bar = 20 µm. **c** Primary apical dendrites of CSMN retrogradely labeled by AAV2-eGFP. Scale bar = 10 µm. **d** Cell bodies of CSMN retrogradely labeled by AAV2-eGFP. Scale bar =

20 μm. **e** Quantitative analysis of apical dendrites reveals significant increase in the average percentage of apical dendrites with vacuoles in the absence of UCHL1. Data presented as mean ± SEM; *$p < 0.05$; **$p < 0.01$; ***$p < 0.001$; one-way ANOVA with post hoc Tukey's multiple comparison test. **f** Quantitative analysis of soma size shows significant reduction in the average CSMN diameter in the absence of UCHL1. Data presented as mean ± SEM; **$p < 0.01$; ***$p < 0.001$; one-way ANOVA with post hoc Tukey's multiple comparison test.

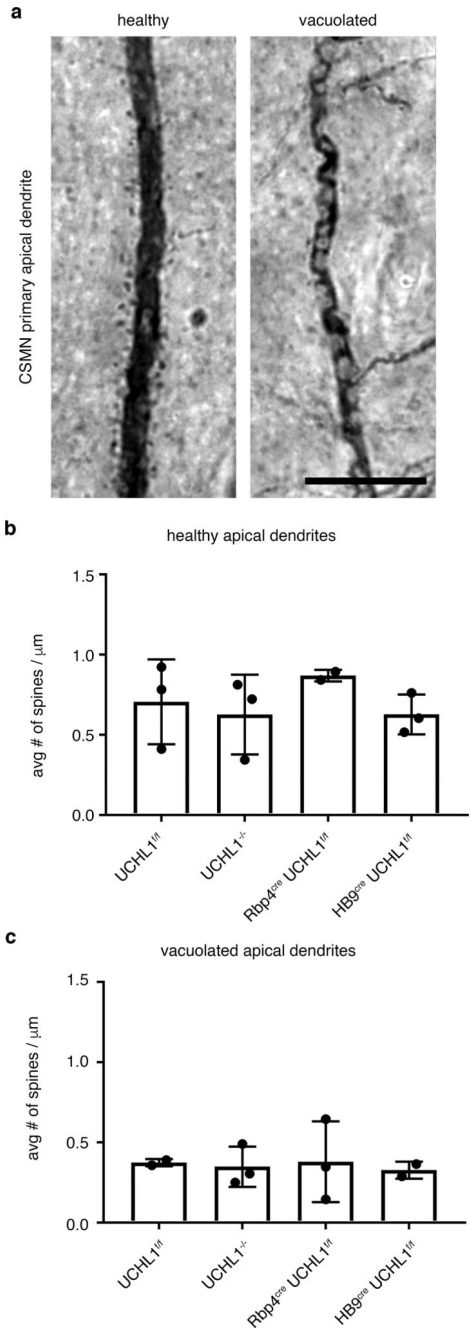


**Fig. 4: Spine density is reduced in degenerating and vacuolated apical dendrites of CSMN.**
**a** Representative images of healthy and vacuolated CSMN primary apical dendrites at P100. Scale bar = 10 µm. **b** Quantitative analysis of average spine density along the primary apical dendrites of healthy CSMN. Data presented as mean ± SEM, one-way ANOVA with post hoc Tukey's multiple comparison test. **c** Quantitative analysis of average spine density along primary apical dendrites of CSMN with vacuoles. Data presented as mean ± SEM, one-way ANOVA with post hoc Tukey's multiple comparison test.

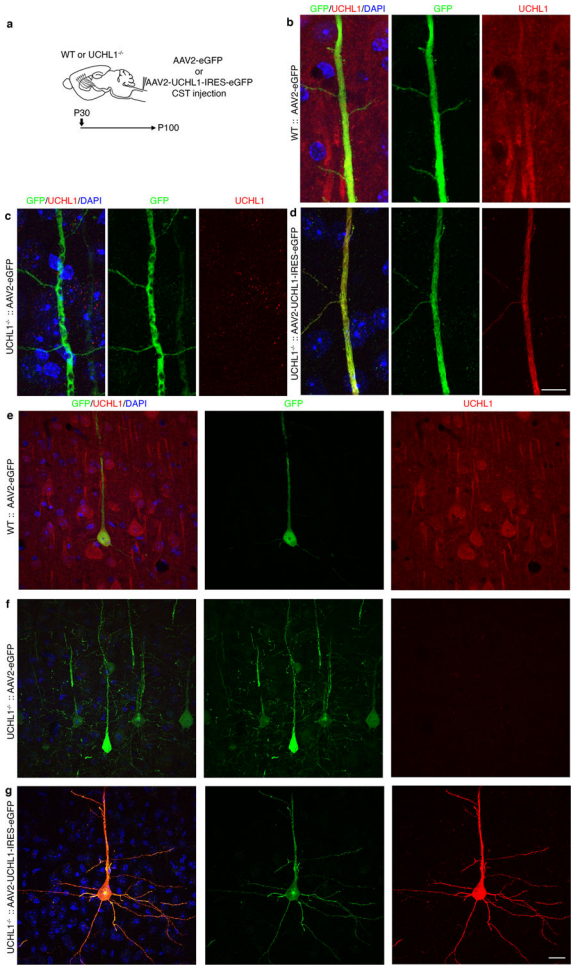


**Fig. 5: UCHL1 expression can be restored in CSMN of UCHL1$^{-/-}$ mice using a AAV2-UCHL1-IRES-eGFP bicistronic expression vector.**

**a** Schematic overview of the experimental setup. CSMN of wild type (WT), or UCHL1$^{-/-}$ mice were retrogradely transduced by injecting AAV2-eGFP into the corticospinal tract (CST) at P30, and CSMN were analyzed at P100. AAV2-UCHL1-IRES-eGFP virus was used for retrograde transduction of CSMN with UCHL1 expression in the UCHL1$^{-/-}$ mice. **b-g** Representative images of CSMN apical dendrites (**b-d**), and soma (**e-g**) retrogradely transduced by AAV2-eGFP in WT (**b,e**), UCHL1$^{-/-}$ (**c,f**) and AAV2-UCHL1-IRES-eGFP in UCHL1$^{-/-}$ (**d,g**) mice. Scale bar **b-d** = 20 μm, **e-g** = 10 μm.

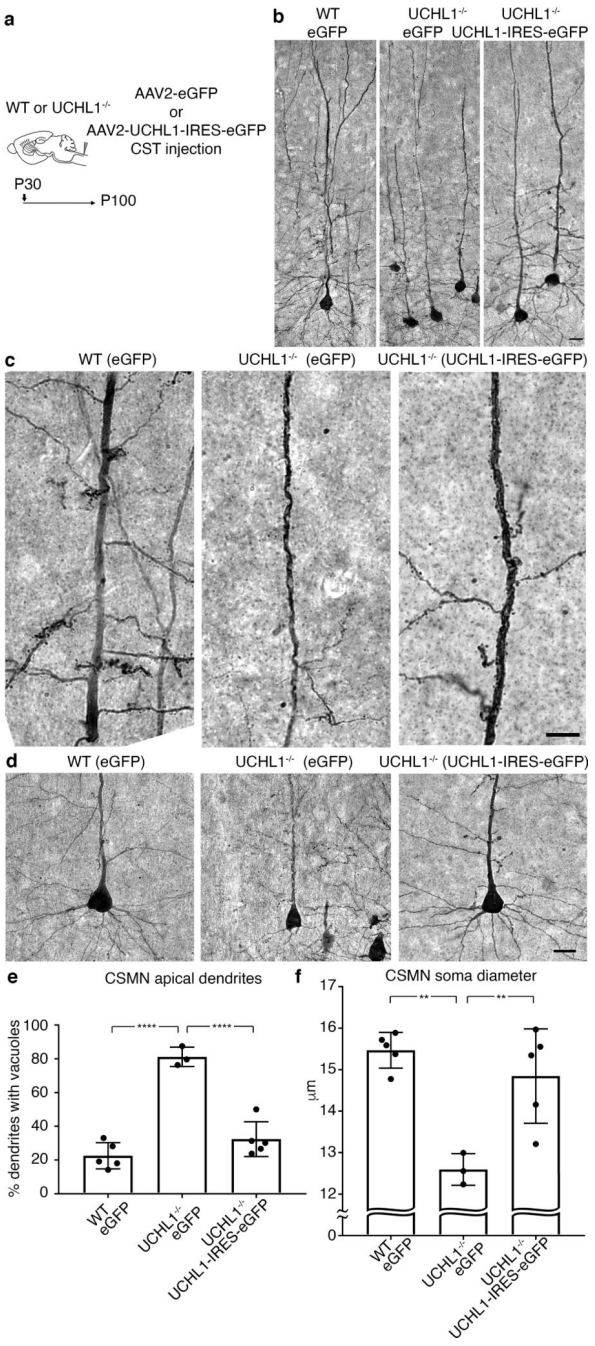


**Fig. 6: Restoration of UCHL1 expression in only CSMN of UCHL1$^{-/-}$ mice is sufficient to improve their health and cytoarchitectural integrity.**

**a** Schematic overview of the experimental setup. CSMN of wild type (WT), or UCHL1$^{-/-}$ mice were retrogradely transduced by injecting AAV2-eGFP into the corticospinal tract (CST) at P30, and CSMN apical dendrites were analyzed at P100. AAV2-UCHL1-IRES-eGFP virus was used to rescue UCHL1 expression in UCHL1$^{-/-}$ mice. **b** Representative images of GFP labeled CSMN after DAB mediated immunohistochemistry enhancement of the GFP signal allowing investigation of CSMN morphology in detail. Scale bar = 20 µm. **c** Primary apical dendrites of CSMN retrogradely labeled by AAV2-eGFP or AAV2-

UCHL1-IRES-eGFP. Scale bar = 10 μm. **d** Cell bodies of CSMN retrogradely labeled by AAV2-eGFP or AAV2-UCHL1-IRES-eGFP. Scale bar = 20 μm. **e** Quantitative analysis of apical dendrites reveals significant decrease in the average percentage of apical dendrites with vacuoles when UCHL1 expression is restored to the UCHL1$^{-/-}$ CSMN. Data presented as mean ± SEM; ****$p < 0.0001$; one-way ANOVA with post hoc Tukey's multiple comparison test. **f** Quantitative analysis of soma size shows significant increase in the average CSMN diameter when UCHL1 expression is restored to the UCHL1$^{-/-}$ CSMN. Data presented as mean ± SEM; **$p < 0.01$; one-way ANOVA with post hoc Tukey's multiple comparison test.

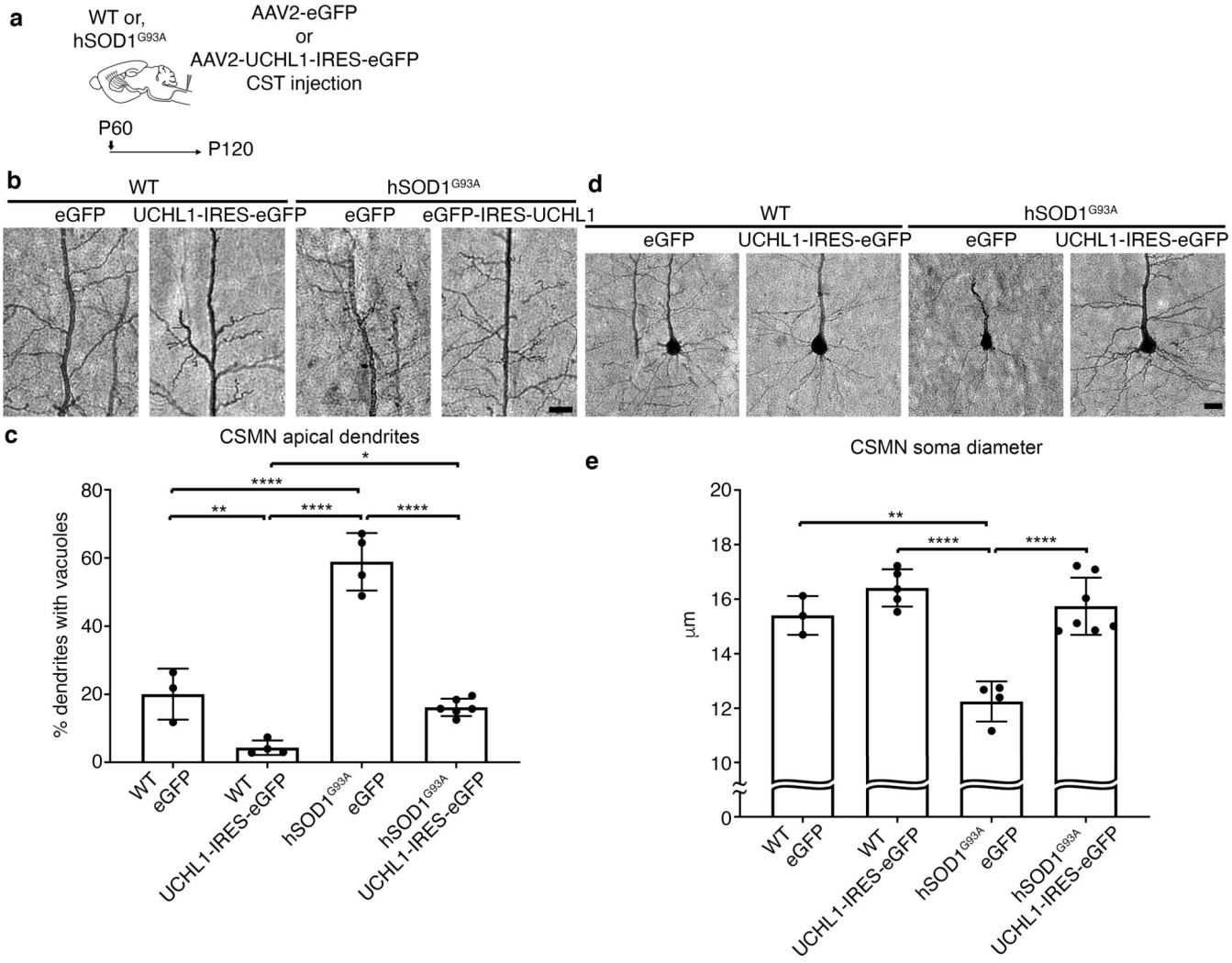


**Fig. 7: Expression of UCHL1 in CSMN of hSOD1$^{G93A}$ mice is sufficient to improve their health and cytoarchitectural integrity.**

**a** Schematic overview of the experimental setup. CSMN of wild type (WT), or hSOD1$^{G93A}$ mice were retrogradely transduced by injecting AAV2-eGFP into the corticospinal tract (CST) at P60, and CSMN apical dendrites were analyzed at P120. AAV2-UCHL1-IRES-eGFP virus was used to express UCHL1 in CSMN of WT, or hSOD1$^{G93A}$, mice. **b** Primary apical dendrites of CSMN retrogradely labeled by AAV2-eGFP or AAV2-UCHL1-IRES-eGFP. Scale bar = 20 µm. **c** Quantitative analysis of apical dendrites reveals significant decrease in the average percentage of apical dendrites with vacuoles when UCHL1 is expressed in CSMN of hSOD1$^{G93A}$ mice. Data presented as mean ± SEM; *$p < 0.05$, **$p < 0.01$, ****$p < 0.0001$; one-way ANOVA with post hoc Tukey's multiple comparison test. **d** Cell bodies of CSMN retrogradely labeled by AAV2-eGFP or AAV2-UCHL1-IRES-eGFP. Scale bar = 20 µm. **e** Quantitative analysis of soma size shows significant increase in the average CSMN diameter when UCHL1 is expressed in CSMN of hSOD1$^{G93A}$ mice. Data presented as mean ± SEM; **$p < 0.01$, ****$p < 0.0001$; one-way ANOVA with post hoc Tukey's multiple comparison test.

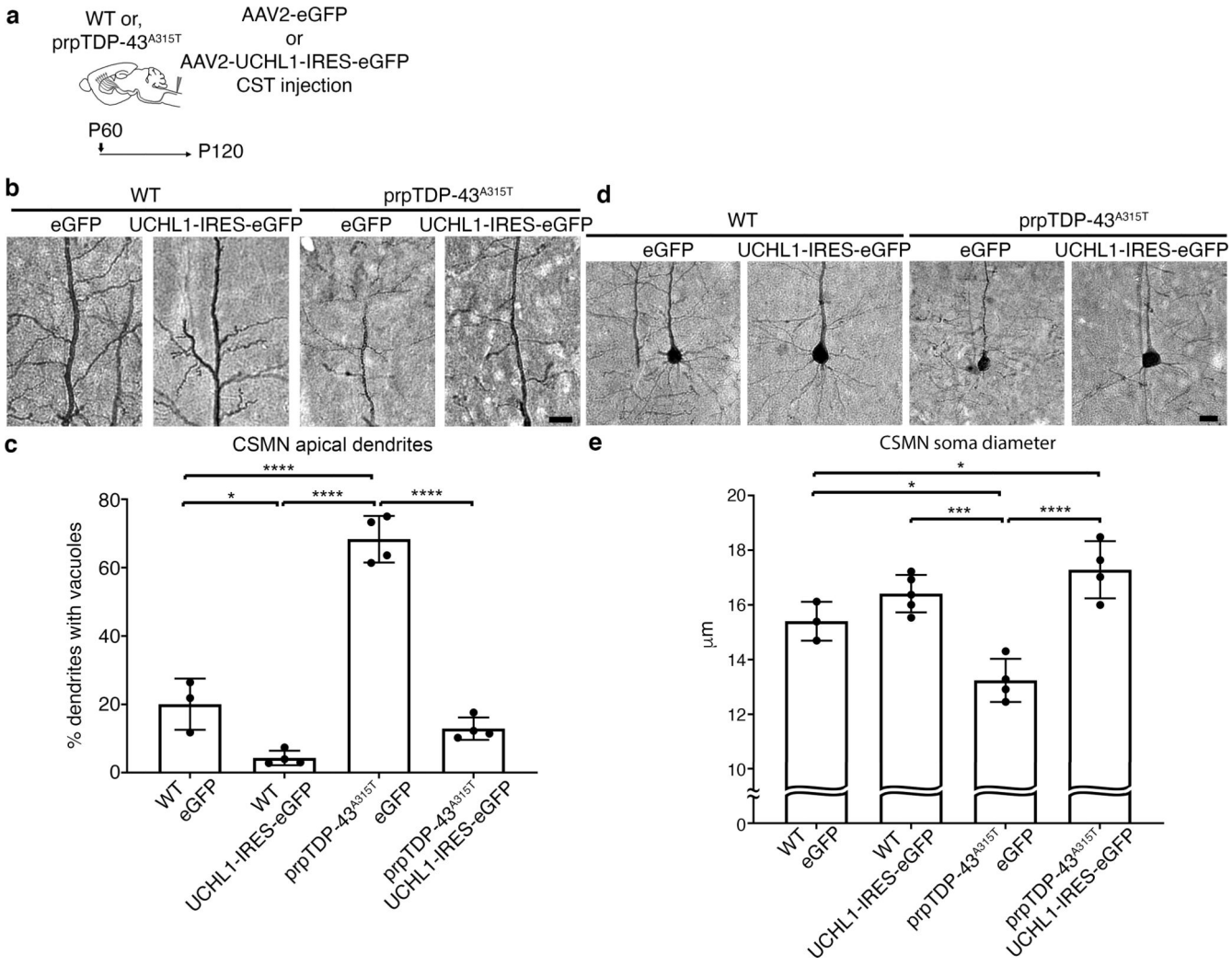


**Fig. 8: Expression of UCHL1 in CSMN of prpTDP-43$^{A315T}$ mice is sufficient to improve their health and cytoarchitectural integrity.**

**a** Schematic overview of the experimental setup. CSMN of wild type (WT), or prpTDP-43$^{A315T}$ mice were retrogradely transduced by injecting AAV2-eGFP into the corticospinal tract (CST) at P60, and CSMN apical dendrites were analyzed at P120. AAV2-UCHL1-IRES-eGFP virus was used to express UCHL1 in CSMN of WT, or prpTDP-43$^{A315T}$ mice. **b** Primary apical dendrites of CSMN retrogradely labeled by AAV2-eGFP or AAV2-UCHL1-IRES-eGFP. Scale bar = 20 µm. **c** Quantitative analysis of apical dendrites reveals significant decrease in the average percentage of apical dendrites with vacuoles when UCHL1 is expressed in CSMN of prpTDP-43$^{A315T}$ mice. Data presented as mean ± SEM; *$p < 0.05$, ****$p < 0.0001$; one-way ANOVA with post hoc Tukey's multiple comparison test. **d** Cell bodies of CSMN retrogradely labeled by AAV2-eGFP or AAV2-UCHL1-IRES-eGFP. Scale bar = 20 µm. **e** Quantitative analysis of soma size shows significant increase in the average CSMN diameter when UCHL1 is expressed in CSMN of prpTDP-43$^{A315T}$ mice. Data presented as mean ± SEM; *$p < 0.05$, ***$p < 0.001$, ****$p < 0.0001$; one-way ANOVA with post hoc Tukey's multiple comparison test.

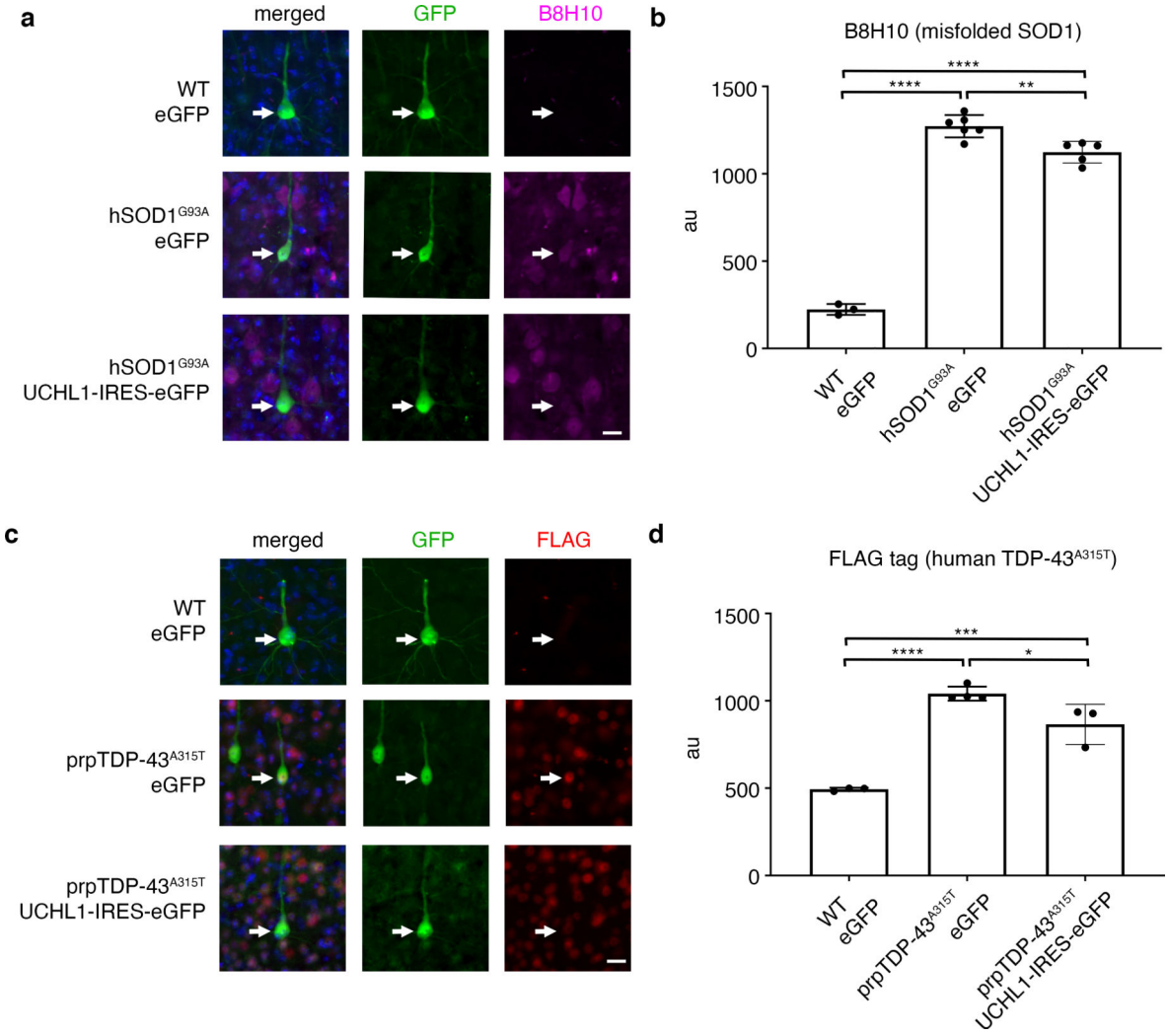


**Figure 9:**

**a** Representative images of CSMN and B8H10 antibody staining that recognizes misfolded SOD1 protein in the motor cortex of WT or hSOD1$^{G93A}$ mice with AAV2-eGFP or AAV2-UCHL1-IRES-eGFP injected into CST. Scale bar = 20 μm. **b** Average misfolded SOD1 fluorescence in CSMN of WT or hSOD1$^{G93A}$ mice with AAV2-eGFP or AAV2-UCHL1-IRES-eGFP injected into CST. **c** Representative images of CSMN and FLAG antibody staining that can be used to selectively visualize the N-terminus FLAG tag attached to the exogenous human TDP-43$^{A315T}$ protein in the motor cortex of WT or prpTDP-43$^{A315T}$ mice with AAV2-eGFP or AAV2-UCHL1-IRES-eGFP injected into CST. Scale bar = 20 μm. **d** Average human TDP-43$^{A315T}$ fluorescence in CSMN of WT prpTDP-43$^{A315T}$ mice with AAV2-eGFP or AAV2-UCHL1-IRES-eGFP injected into CST. Data presented as mean ± SEM; *$p < 0.05$, ***$p < 0.001$, ****$p < 0.0001$; one-way ANOVA with post hoc Tukey's multiple comparison test.